REVIEW

Microfluidic Organ-on-a-Chip Technology for Advancement of Drug Development and Toxicology

Jeremy D. Caplin, Norma G. Granados, Myra R. James, Reza Montazami, and Nastaran Hashemi*

In recent years, the exploitation of phenomena surrounding microfluidics has seen an increase in popularity, as researchers have found a way to use their unique properties to create superior design alternatives. One such application is representing the properties and functions of different organs on a microscale chip for the purpose of drug testing or tissue engineering. With the introduction of "organ-on-a-chip" systems, researchers have proposed various methods on various organ-on-a-chip systems to mimic their in vivo counterparts. In this article, a systematic approach is taken to review current technologies pertaining to organ-on-a-chip systems. Design processes with attention to the particular instruments, cells, and materials used are presented.

1. Introduction

Before a new drug is released in the market it must go through intensive testing; prior to approval for human testing, most drugs first need to be tested for safety through animal testing. The use of animals in such experiments is often expensive, time consuming, ethically controversial, and is often an inaccurate representation of actual human response.[1] Two-dimensional cell culture models are also not the best solution because the cells do not respond the same way when their surrounding environment is drastically different from that of a human body.[2] Organ-on-a-chip technology provides a practical solution to many of the issues presented by both two-dimensional models and animal testing. An organ-on-a-chip is a cell culture model with microfluidic channels[3] configured such that it is capable of simulating the activities and physiological responses of an entire organ.[4] This type of device creates a uniquely accurate method for replicating the organ structure of human tissue and observing the biological responses, as opposed to predictions based on extrapolated data from animal testing. The

chip is portable, requires little amounts of materials, creates a small footprint, and is cost effective, making its applications limitless.[5] With some more improvements and careful testing, this technology may be able to help drugs get into the market faster, increase the number of new drugs investigated, and possibly eliminate animal testing altogether.

Many "organ-on-a-chip" devices have already been made.[6] For example, the Wyss Institute at Harvard have fabricated a "lung-on-a-chip", which is mainly made of three microfluidic channels, with the center one holding a porous membrane on which alveolar epithelial and vascular cells are grown.[7] A breast-on-a-chip has also been developed to study tumor nanoparticles for identifying and treating tumor cells.[8]

The next step for this technology is to connect various organ-on-a-chip devices to one another to create a "body-on-a-chip." This configuration could possibly allow researchers to investigate the effects of substances not only on the individual organs but to replicate the interactions between each component, providing a more comprehensive analysis which could ultimately revolutionize how drugs are developed.

2. Microfluidic Organ Types and Functions

2.1. Liver

The approval of introducing new drugs to the market has proven to be a difficult barrier to overcome due to the risks associated with them. As the cost of bringing a new drug into the market keeps rising in the United States, there becomes a larger need to have high performance pre-clinical drug screenings using in vitro models. The liver has proven to be one of the most difficult organs for drug approval, due to the strong interactions it has with other organs, as well as its sensitivity to the metabolism of certain drugs.[9] This leads to a high percentage that are discontinued and removed from the market. Technologies to study microvascular structure and functions have remained largely unchanged since the late 1970's. Improving the systems and technology used to test for toxicity is key to providing better predictions of toxicity and ensuring the safety and efficacy of new drugs well before they reach market.[10] There has been a considerable amount of research done in the area of toxicity testing on organs, with hopes to fabricate a simpler, efficient,

J. D. Caplin, N. G. Granados, M. R. James,
Prof. R. Montazami, Prof. N. Hashemi
Department of Mechanical Engineering
Iowa State University
Ames, IA 50011, USA
E-mail: nastaran@iastate.edu
Prof. R. Montazami, Prof. N. Hashemi
Center for Advanced Host Defense Immunobiotics and Translational
Comparative Medicine
Iowa State University
Ames, IA 50011, USA

www.MaterialsViews.com

ADVANCED
HEALTHCARE
MATERIALS

www.advhealthmat.de

REVIEW

effective, and accurate microfluidic system mimicking the functions of the liver.

Cells used to represent the liver primarily consist of hepatocyte cells, due to their uncanny ability to mimic liver functions.[11] Research has taken advantage of this trait in order to produce a working liver-on-a-chip design.[12] Toh et al.[13] created a system that can also address the cell culture chamber independently, so that different drugs concentrations can be simultaneously increased. The 3D microfluidic cell culture system, dubbed the "3D HepaTox Chip," is designed to support 8 parallel channels containing separate cell cultures, with a linear concentration generator to provide different levels of drug concentration to each channel. An array of micropillars (30 µm × 50 µm) separate the cell culture channel into three compartments consisting of a 200 µm wide central culture with two side compartments. The central culture had the purpose of keeping a constant cell suspension, while the side compartments introduced flow from the output of the concentration generator. To assess the functionality of the cell culture, albumin production and various metabolic activities were measured. Results showed that this microfluidic model was equally capable of the functional maintenance of the hepatocytes as a multi-well plate model, if not more so. The hepatotoxicity testing was performed using five model drugs: acetaminophen (20 mM), diclofenac (1000 µM), quinidine (1000 µM), rifampin (2000 µM) and ketoconazole (420 µM). Results showed that the cells were more sensitive to the drug-mediated hepatotoxicity than the multi-well plate cultures. The toxicity data also showed a positive correlation with comparable in vivo toxicity data.

While some researchers focus on using 3D microfluidic devices for toxicity testing, others have focused on functionality. Nakao et al.[14] developed a microfluidic cell culture device that mimics the microscopic structure of the hepatic cords. Due to the decline in liver specific functions caused by freshly isolated hepatocytes rapidly losing their membrane polarity, a new technique for maintaining the cells was proposed, in which hepatic activity was prolonged by suctioning the cells into the cord-like compartment of the device, creating a "collagen sandwich culture". The design is such that the tip of this compartment has an asymmetrical tip that can house two cells side-by-side. Current liver tissue cultures do not a have separate compartment to collect secreted bile and are accumulated in the cultured cells. However, in vivo, the bile is excreted into the bile canaliculi and is then discharged into bile ducts. The area of culture was formed by aligning two lines of hepatocyte cells in a similar way to the hepatic cords. The aligned hepatocytes were able to self-organize themselves and form bile canaliculi along the hepatic cord-like structure. The device has a medium flow channel that is 100 µm wide and 30 µm high, a cell loading channel that is 200 µm wide and 30 µm high, a cell culture area that is 37 µm wide and 30 µm high and an endothelial-like barrier. Additionally, there are 30 µm long narrow slits with 10 µm intervals that allow the nutrition to go into the cell culture area. The fluorescent substrates accumulated in the cells were aligned and formed a bile canaliculi with tight junctions. This bile canaliculi showed the ability to utilize nutrients in the culture medium stream. Additionally, using the MRP2 and CD147 marker proteins, the transportation properties of the system were tested, and the markers were found to be distributed in a similar fashion as they would in an in vivo counterparts.

Incorporation of biosensors has also been studied as a means to create improved analysis of a system, in addition to the development of the microfluidic platform. As part of the construction done by Schober et al.,[15] AlGaN/GaN nanosensors were integrated into their microdevices, and were used for optical monitoring of the cells. The design consists of a base and top module used for the purpose of carrying the cell culturing substrate; within this contains a microfluidic pumping system used for circulation and perfusion. The cultivated cells are contained in a polymer scaffold system, called "MatriGrid." The hepatoma cell line, HepG2, demonstrated the biological application of the microreactor. Analysis was done for 2D cell culture, 3D culture without perfusion, and 3D culture with perfusion. Tests for viability were completed and analyzed for the cells cultured in the 2D and 3D systems over a course of 19 days. All three cultures showed a similar general relationship between the $G_{1,0}$, D, and $G_{2,m}$ phases, with the 2D culture displaying a higher proliferation rate than what is typically seen in vivo. The notable difference came from monitoring the albumin secretion of the cultures. Albumin secretion was used as a metabolic marker to observe the similarities between the cultures used during the experiment and the in vivo counterpart. Results showed that only the 3D culture without perfusion strayed from predicted results, showing a notable increase in production over time. Additionally, the system with and without HepG2 cells went through pH testing. The results showed a steading increase in pH for the system with HepG2 cells, and a relatively unchanged pH for the system without. This is due to the conversion of glucose to lactate that occurs in vivo as well. These results showed a strong signal with little noise, showing reliability that can be applied for long-term monitoring of cells. Their perfused bioreactor system mimics some of the features that are found in vivo as well.

Lee et al.[16] designed a microfluidic device that contained polyethyleneglycol (PEG) pillars within a weaving channel, with each pillar containing rat liver microsomes enclosed within a 3D hydrogel matrix. The pillars took up around 35% of the space within the channel and were roughly spaced 100 µm from each other. Gravity induced flow was able to mimic the metabolism reaction and the transport system of the liver. The concentrations of seven different substrates were used to test the P450 reaction in a microsome solution within a standard well plate system, ranging from 2 µM to 80 µM. Two trials were conducted: one in which the microsomes were in the solution phase by themselves and another in which the microsomes were enclosed within the 3D matrix. Data was extrapolated and a mathematical model of the system based on Michaelis-Menten kinetics was produced, showing a high level of agreement between the two. The chip was then analyzed and a model was created. This model also showed a high level of agreement. However, ideal assumptions were created to simplify the model, including: no variation in the z-axis, completely effective diffusive properties within the channels, a completely homogeneous environment (a single diffusion coefficient), and a uniform reaction space within the channel. Certain steps still need to be taken to improve the model, like improving the diffusive properties and convective flow rate of the device, but the success of

REVIEW

the model shows that the metabolic properties within a microfluidic liver model can be mapped and understood to create an experimental equivalent for use in liver-on-a-chip applications.

While the use of a single cell culture has shown to yield successful results, using multiple cells in a liver-on-a-chip model has the potential for even more realistic in vitro results due to the livers true complex nature being composed of multiple cells in interaction with each other. This line of research has produced notable results as well.[17] Schütte et al.[18] used this approach, in addition to developing a microfluidic test system for liver toxicity. This system is an organ-like liver 3D co-culture of hepatocytes and endothelial cells. The chip allows for the assembly of primary human hepatocytes and endothelial cells in a sinusoidal-like manner with the use of dielectrophoresis (DEP). The system was integrated with microfluidic channels that allowed for continuous perfusion of the culture medium and compound testing. The features within the channel structure are comprised of electrodes at the outer chamber walls with a variation of the channel cross-section in between. Micro pillars were attached to the front and back ends of the gaps to represent flow barriers, which reduced the flow velocity and shear forces. The device was connected to a pump system for fluid control with AC voltages of up to 300 V_{pp}. Each design had a gap region 100 µm high, 100 µm wide, and 1500 µm long, as well as a 33° angle of inclination on the bottom channel so that particles traveling along the bottom can still be lifted into the gaps by dielectrophoretic force (**Figure 1**a). The device only trapped the healthy living cells, thereby resolving a problem of the past. Once the electric field was turned off, the cells showed a more even distribution, with the hepatocyte cells in the center and the endothelial cells outside of them (Figure 1b). This distribution was sufficient enough to not be affected by the flow.

Another multi-cell design was created by Wagner et al.,[19] who designed a multi-organ chip (MOC) platform that combined a microfluidic channel system with multiple separate tissue culture compartments. Liver micro tissues (HepaRG and HHSteC), as well as skin biopsies, were combined and had
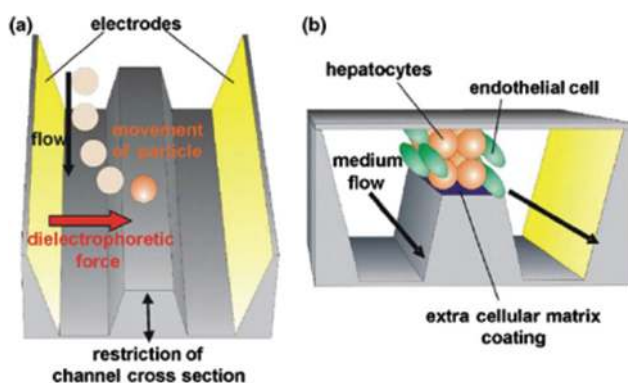

Figure 1. Cross section of the microchannel displaying the general layout. a) Two electrodes are positioned at each wall of the channel, providing a dielectrophoretic force to the hepatocytes and the endothelial cells traveling along with the flow once voltage is applied to the system, with the design of the device such that the particles are maintained in the center. b) Once the voltage is shut off, the particles are arranged such that the endothelial cells are positioned outside of the hepatocytes, while still being somewhat maintained in the center of the channel. Reproduced with permission.[18] Copyright 2011, Springer.

successful long-term performance. The device contained microchannels and micropumps, as well as culture compartments for Transwell inserts. The system allowed crosstalk between the two tissues, and was observed for 14 days while exposed to fluid flow. Consistent disk-shaped liver cells were formed during 2 days of having been cultured on the chip. The microchip device was able to culture two cell types while directly exposed to fluid flow, as well as maintain a metabolic steady state. It is able to culture and maintain cells over longer periods of time with the Transwell inserts as the system showed it could be maintained for 28 days.

Additionally, multiple toxins can be used as well to increase the scope of the experiment. Shintu et al.[20] developed a microfluidic system with H NMR-based metabolomic foot printing. They used a small-molecule screening approach to characterize the toxicity in several compounds: ammonia (NH_3), dimethylsulfoxide (DMSO), and acetaminophen (APAP). Hepatocellular carcinoma cells (HepG2/C3A) were used to model the liver, Madin-Darby canine kidney (MDCK) tubular epithelial cells to model the kidney, and a combination of both (HepG2/C3A-MDCK) as cell co-cultures. When the biochips are perfused, the supply of nutrients is restored, the cells proliferate, and a higher glucose and glutamine consumption is seen. HepG2/C3A is correlated with higher glucose concentrations and lower lactate and alanine concentrations when compared to the MDCK kidney. Additionally, the co-culture showed unique metabolite concentrations not expressed in any of the single cultures. This information was used to control these differences to ensure that they have the same "starting point" with relation to their reaction with the compounds. A data-scaling method known as "SMART-scale analysis" was used to account for these differences. Using this method, the relative increase and decrease of metabolic markers was analyzed. These fluctuations, both alone and in combination with one another, can create results in various biological processes, including toxicity production. An "integrated knowledge network" was created to map out these biological processes and their implications. From this, the actions from the metabolic markers can be observed for toxicity screening purposes. Experimental results were conducted and the metabolic responses were observed and compared alongside the theoretical data. The results showed a high degree of compatibility for all three compounds.

Integrating tissue slices is another technique used by researchers to create an in vitro co-culture model.[21] Van Midwoud et al.[22] investigated whether intestinal tissue slices could also be cultured in a micro biochip with liver slices and also to see if their metabolic activity in incubation is better than in the well plate system. The intestine, as well as the liver, is important for the metabolism of xenobiotics. The liver and intestinal slices were obtained from male Wistar rats. They exposed the substrates to several mediums: 7-ethoxycoumarin (7-EC), 7-hydroxycoumarin (7-HC) and lidocaine (Li), to see if their metabolic rates in the biochip were similar. The slices were also exposed to a primary bile acid, chenodeoxycholic acid (CDCA), to see the interplay between the two organs. One slice of liver and one slice of intestine were placed into a compartment culture perfusion system with a continuous flow of the mentioned mediums. The microdevice itself had 10 layers of polydimethylsiloxane (PDMS), which each had a thickness of 250 µm and

along with 6 microchambers. The device had a medium top/bottom inlet channel that was 500 µm × 100 µm, and a polycarbonate filter that had 8 µm size pores and 10µm in thickness integrated at the entrance of the tissue chamber. The filter was 4 mm × 2 mm and held 25 µL. It was found that it is possible to successfully maintain intestinal slices in the same biochip with viability and functionality for at least 3 h. With this system they were able to easily control the flow of the medium and transfer it from one organ to another. It was also possible to link one microchamber to another for the use of perfusion and metabolic activity. They were able to integrate the liver and intestine, and it could potentially work for lung, kidney, and colon slices.

Just like van Midwoud et al., Bricks et al.[23] developed a model to mimic the interactions between the intestine and liver. However, instead of using actual slices of the organs, they used the human carcinogenic epithelial cell line Caco-2 TC7, which is the clone of Caco-2 cells, for the intestine, and hepatocarcinoma HepG2/C3A cells for the liver. A new microfluidic device called the Integrated Insert in a Dynamic Microfluidic Platform, or IIDMP, was used to evaluate the organ–organ interactions of the liver and intestine. This design consisted of 3 perfusion units, each unit containing two wells used as reservoirs, one cell culture insert, and one microfluidic chip that was made of PDMS. The insert was contained within the first well, with circulation traveling through the bottom of the first well into the second well, by means of a microfluidic chip bridging the two wells. A pump was used to bring flow from the second well back into the first well, thereby completing the cycle. The Caco-2 TC7 cells were cultured in the insert, while the HepG2/C3A cells were cultured in the microfluidic chip. Both cells were individually tested for integrity and functionality before integration into the system. Confluence of Caco-2 TC7 cells were found using transepithelial electrical resistance (TEER) measurements and permeability properties were found by monitoring Lucifer yellow transportation. Results showed high levels of both after sufficient time within static culture, suggesting that the system gained tight junction properties, which is in agreement with expected results. Dynamic conditions proved to produce similar results. HepG2/C3A cells were cultivated and the functional properties were tested in both dynamic and static conditions. Dynamic conditions were tested with and without the influence of Caco-2 TC7 cells in the system. Albumin production was reported to be non-existent in the static culture, while producing higher values with the influence of Caco-2 TC7 cells compared to the system without them, despite the fact that the Caco-2 TC7 cells showed no production of albumin themselves. Bricks et al. proposed that this was due to a stimulating effect that the Caco-2 TC7 cells have on the HepG2/C3A cells. The xenobiotic metabolism was tested using the EROD test. The enzyme CYP1A was chosen for monitoring. Results showed low levels of activity when compared to primary hepatocytes, with dynamic trials showing no metabolism after 24 hours and static trials showing no activity at all after 24 h. The co-culture of Caco-2 TC7 cells and HepG2/C3A cells were then tested by monitoring the CYP1A activity when the drug phenacetin was introduced to the system. Both static (Petri) and dynamic (IIDMP) were evaluated. The resulting APAP production was observed to be higher in the dynamic culture, despite the fact that the hydrophobic properties of phenacetin may have led some of it to be absorbed into the PDMS components of the IIDMP. When dynamic conditions with and without Caco-2 TC7 were tested, the system with Caco-2 TC7 once again produced greater amounts of production. This experiment reaffirms the hypothesis that integration of tissues from multiple organs creates a more realistic in vitro model due to both the simple connections and the underlying influences they have on each other.

2.2. Lung

In response to the lack of experimental model systems available that can accurately replicate human lung response and function, many are currently researching and developing new technologies. The microdevice, lung-on-a-chip, recapitulates the physiological and mechanical microenvironment of a living lung. This technology allows for the study of complex physiology of the human lung. With the aid of organ-on-a-chip technology, new drug therapies can be developed, respiratory assist devices can be utilized, and pulmonary diseases can be characterized.[24]

In early work by Huh et al.,[25] a microdevice was developed which allowed for the analysis of the effects of liquid plug flows on human small airway epithelial cells (SAEC). The device consisted of two PDMS layers containing a microfluidic channel separated by a nanoporous membrane, modeled after the human airway epithelium. Additional inlets and channels were created to connect a liquid plug flow generator. Liquid plug flows were created using a device that would switch the air-liquid interface within the chip, as shown in **Figure 2**. Through this device, the effects of an air intake model (useful for representing a healthy lung), fluid intake model (useful for representing the developing lung of a fetus), and a variable length two-phase plug flow model (useful for representing respiratory diseases such as pulmonary edema) on the cells can be monitored as the system operates. Small airway epithelial cells were first cultured in a culture media on the membrane until a confluent layer was formed, then exposed to air in the culture chamber. Using a laser vibrometer, the magnitude of the pressure waves from the liquid plug flows was measured. The Weibel model was used as a reference for the size and speed of the plug flow. At a rate of 1 plug per minute, the results showed that only 24% of the cells survived after 10 min, with most damage occurring downstream where the plug erupted. This result shows the capabilities of lung-on-a-chip devices for representing pulmonary diseases in a microfluidic platform.

In a similar experiment designed to study the damage of lung cells by recreating liquid plug flow, a microfluidic device was developed by Tavana et al. to monitor the induction of pulmonary pressure on the culture system.[26] While the device shows a similar design to the previous design by Huh et al. for the integration of the liquid plug and the culture chamber, this project is designed to look at the role that surfactants play in the damage of lung cells. Deficiencies of pulmonary surfactants occur from the destabilization of liquid lining of small airways causing osculating liquid plugs. In vivo, this is prevented by the secretion of a liquid surfactant from the alveolar epithelial cells. Human alveolar epithelial cells were used for the model, and
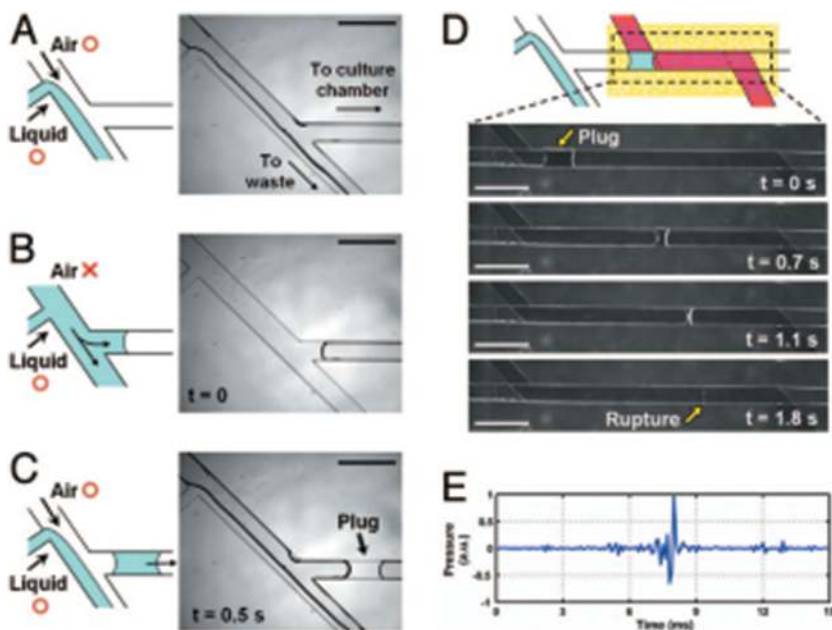
Figure 2. Process of creating the liquid plug for the microsystem. A) The process begins with air being produced in the upper inlet and liquid being produced in the lower inlet. Liquid is flowing from the lower inlet into the waste stream, so that the only fluid within the culture chamber is air. B) The plug is started once the upper inlet is blocked, bringing liquid into the culture chamber. C) The plug is complete once the upper inlet is reopened and the liquid from the lower inlet is once again only flowing into the waste stream. D) A complete picture of the plug system and the microfluidic chip can be seen, with the actual chip being highlighted in yellow. The plug will slowly dissipate as it travels through the chip until it ruptures, E) releasing pressure waves in the system that can be monitored. Reproduced with permission.[25] Copyright 2007, National Academy of Sciences.

cultured in F-12K medium. An air tank was used to supply air and a syringe pump was used to supply liquid. Size and duration of the plug flow was determined using a pressure transducer controlled by a DAQ board. During the experiment, the microchip was placed on a glass slide and observed on a microscope. Cells were stained with CellMask Deep Red plasma membrane stain to monitor the effects of the liquid plugs. The cells were imaged using an inverted florescence microscope. A surfactant-free trial was run on the device, showing extensive injury to the lung cells. The surfactant, Survanta, was then introduced at 1 mg per ml of buffer for the next trial. Results showed a major decrease in the percentage of cell injuries in the system. For comparison, the surfactant-free trial showed a cell viability of 63% after three plugs, whereas the surfactant trial showed a cell viability of 81% after five plugs. This in vitro pulmonary airway platform can be used to study cellular and sub-cellular effects in airway reopening.

Built on the work of his previous design, Huh et al.[7] designed and fabricated a biomimetic microsystem in 2010 to not only mimic the cellular and diffusive properties of the lung, but also the macroscopic behavior, such as the expansion and compression of the system to mimic inhaling and exhaling. The microfluidic system consisted of two microchannels that were separated by a membrane of polydimethysilxane (PDMS), as opposed to a membrane of polyester in the earlier design. This lung-on-a-chip system is capable of mimicking the human lung's response to bacteria and inflammatory cytokines. The membrane was coated with ECM and human alveolar epithelial cells (NCI H441), and human pulmonary microvascular endothelial cells were cultured on the opposite side of the membrane (**Figure 3**A). Two hollow mirochannels on either side of the flexible membrane acted as vacuum chambers to simulate breathing movements (Figure 3C–E).
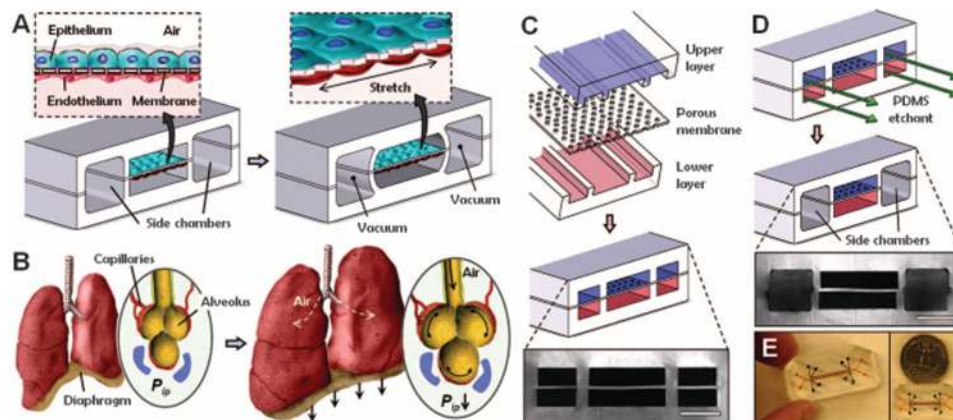

Figure 3. Design layout for lung-on-a-chip, showing A) a cross-sectional view of the device. Human alveolar epithelial cells are cultivated on the top of the membrane, while human pulmonary microvascular endothelial cells are cultivated on the bottom of the membrane. B) A view of the human lungs, showing the stretch and the resulting distribution of the air intake during the inhalation portion of the breathing cycle. C) The device consists of two PDMS layers with a porous membrane separating them. D) Once the layers are sealed, an etchant flows through the vacuum chambers. E) The finished design of the chip, with a quarter for scale. Reproduced with permission.[7] Copyright 2010, American Association for the Advancement of Science.

This design took advantage of the flexible PDMS membrane to better recreate physiological breathing (Figure 3B). Through the study they also found that due to the mechanical strain of air being pulled in and out of the lung, the epithelial and endothelial uptake of nano particulates were enhanced and stimulated their transport into the underlying microvascular channel. To test their device, bacteria and inflammatory cytokines were introduced into the air, and human bloodborne immune cells were introduced into the blood-like fluid. It was observed that the lung-on-a-chip can mimic the innate cellular response to pulmonary infection of bacterial origin. However there are still differences between in vivo and the device, such as changes in air pressure and flow, cellular composition, and barrier thickness, that still need to be accounted for before it becomes a reliable alternative to animal testing.

The work done to mimic pulmonary edema in a human disease model-on-a-chip was expanded by Huh et al.[27] in 2012. The devices used in the study were slightly modified from previous work.[7] Once again PDMS was used as the top and bottom layers of the chip. The side chambers were created by etching the membrane layers in the side microchannels with tetrabutylammonium fluoride and N-methylpyrrolidinone, mixed at a ratio of 1:3. The solution was introduced into the side microchannels through inlet reservoirs by either hydrostatic pressure or vacuum suction. Etching took place until the thickness of the PDMS walls between the side chambers from the central culture chambers became thinner than 30 µm. Afterwards, the side chambers were washed with NMP to remove any PDMS etchant that remained. After the alveolar epithelial cells were attached to the upper alveolar channel, culture media flowed through the device at 50 µL h^{-1}. Cells were grown for 5 days; on day 5 the culture medium was aspirated from the upper channel and a 50:50 mixture of epithelial and endothelial medium was introduced into the lower channel. This fed the alveolar epithelial cells on their basolateral side. For 15 days, epithelial cells were grown at an air-liquid interface. Just as in the previous device,[7] the upper alveolar channel was filled with air and the lower microvascular channel was filled with liquid. Additionally, a vacuum was connected to the system to mimic breathing motion as a functioning human lung. It was shown that with the addition of cyclic mechanical strain to IL_2, leakage increased dramatically. The drug DSK2193874 was tested and shown that it could inhibit leakage. This demonstrates an additional step towards mimicking lung functions, and brings research one step closer to successfully predicting the activity of a new drug for cases involving pulmonary edema. The goal of having the ability to rapidly screen many drugs and conditions could one day become a reality once models can be connected to many other organ-on-a-chip models. This could bring about a more accurate representation of how pharmaceuticals affect all areas of the body.

Other mechanical properties were explored by the microsystem created by Douville et al.,[28] who observed the effects of both solid and fluid mechanical stress on alveolar epithelial cells with a ventilator-induced lung injury (VILI). The device consisted of three major components: the alveolar chamber, PDMS membrane, and actuation channel. Human alveolar basal epithelial (A549, AEC) cells were cultured in this model. The main contributor to solid mechanical
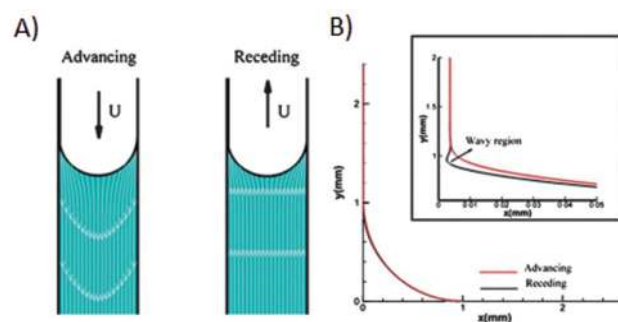

Figure 4. Monitoring and computational fluid dynamic (CFD) analysis on the mechanical stresses of an advancing meniscus fluid plug versus a receding meniscus fluid plug. A) The streamlines of both menisci are displayed, with $U = 1$ cm s^{-1}. B) The half-meniscus profile was calculated and graphed. The results show a smooth profile for the advancing meniscus (red), while the receding meniscus (black) contains abnormalities when focused on the edge of curvature (exaggerated display is boxed) that will increase the stress applied on the cell layer. Reproduced with permission.[28] Copyright 2011, The Royal Society of Chemistry.

stress for VILI is the cyclic stretching of the cells, while the main contributor to fluid mechanical stress is an air-fluid meniscus. Advancing versus receding menisci were observed for their stress impact as well (**Figure 4**), with the confirmation that a receding meniscus causes more harm to cells than an advancing one. A finite element analysis (FEA) model was used to estimate the solid mechanical stress and the resulting model was proposed as a means to estimate the stress profile by measuring the maximum deformation of the system. Results showed a viability of 16.8% in the A549 cells and 32.5% in the AEC cells when exposed to both solid and liquid mechanical stress. This study prompts further research on understanding techniques to eliminate hazardous stresses in clinical settings.

While these designs have improved the functionality of an in vitro lung design, a major problem with these designs is their poor permeability when compared to an actual working lung. This issue was addressed by Kniazeva et al.,[29] who created a microfluidic design to maximize gas transfer, with the goal of working towards creating an artificial lung or a lung assistant device. The design consisted of a small branched network of channels representing the microvascular system, with an ultrathin membrane separating the microvascular network from the channel representing oxygen flow. This design is repeated to create a multi-layer design with alternating levels of microvascular channels and oxygen channels. The ultrathin gas exchange membrane is used to maximize gas transfer efficiency while minimizing membrane-blood contact area, which is one of the main challenges in artificial lung technology. The network is designed to minimize blood damage, thrombosis, and inflammatory responses. The microvascular network also provides controlled wall shear stress and uniform blood flow. The device addresses many limitations seen in lung assist devices such as the Extra Corporeal Membrane Oxygenator (ECMO). Current ECMO devices have surface area to volume ratios that are 10 times less than the natural lining of a human lung. Additionally, the gas diffusion distance in the ECMO is 10–30 µm greater than the 1 µm observed in the natural lining.

ADVANCED
HEALTHCARE
MATERIALS

www.advhealthmat.de

Materials
Views

www.MaterialsViews.com

REVIEW

Leaks of proteins, phospholipids, and lipoproteins often occur, which cause device failure. ECMOs also use non-physiological blood flow pathways that can be unpredictable and uncontrollable. The membrane used in this device is thinner than the membranes used in ECMO devices, thus less surface area is required for equivalent oxygen transfer and the membrane is more gas permeable. Two different methods were used to test the device. The first test characterized the permeance of the PDMS membrane in a static medium. The second test analyzed oxygen transfer through the membrane. It was found through experiments that as the membranes became thinner, the permeance increases. The relationship was modeled with the equation:

$$K = Q_2 / SA \cdot \Delta P \qquad (1)$$

where K is the permeance, Q_2 is the actual oxygen flow rate, SA is the surface area of oxygen transfer (was the same for each device), and ΔP is the transmembrane pressure. Following Equation (1), it was found that K stayed relatively constant at a given membrane thickness. Therefore, as the transmembrane pressure doubled, the flow rate also doubled. The bilayer subunits that make up this device are easily reproduced and can be connected in different configurations. Membrane thickness can also be controlled and optimized. It was found that by using thinner sheets to create channels, overall oxygen transfer was increased. This device will be useful in artificial lung and lung assistant device applications that require high transfer rates of oxygen.

Many lung assist devices today are limited to care unit settings because they are not implantable or portable. From this, lung assist microdevices that utilize vascular networks are being designed, with the hopes that they can be implanted in the patient.[30] Sreenivasan et al.[31] developed a lung assist device that is designed to achieve physiologic flow through utilizing microfluidic vascular networks, which may allow this device to be implanted if it is impermeable to fluid. Sreenivasan et al. aimed to improve their previous 8 µm silicon membrane by designing the gas exchange membrane to be more permeable. They designed and developed a free-standing membranes (FSM) and composite membranes (CM) by means of initiated chemical vapor deposition (iCVD). A control membrane of 8 µm thick spun cast silicone was used to compare the two designs. Both devices were also tested for bond integrity. Sreenivasan et al. chose to work with p(nBA) and p(tBA) based chemicals for free-standing membranes due to their ability to withstand bonding. The p(AA) was spun at 4000 rpm for 40 s then baked at 150 °C for 2 min to create a sacrificial layer. The p(AA) would then dissolve away, leaving the FSMs. The FSMs successfully remained intact during handling. The FSM with a thickness of 5 µm expressed a CO_2 permeance 1.3 times higher than the control membrane. An alternative to ultrathin FSMs are composite membranes. CMs are composed of a highly permeable porous structure coated with a skin of a secondary polymer. These 0.1 µm commercially available membranes provide mechanical stability to the device and minimize the chances of membrane rupture. The top skin layer allows gas transfer, while acting as a separation for liquid and gas. The CMs expressed CO_2 and O_2 permeance of 50–300 times

the control membrane. These CMs are on the right track to achieving the permeable membrane needed for portable lung assist device. Defect-free thinner membranes (20–500 nm) are currently under development.

Microfluidics can also be applied for the characterization of cellular responses, such as the correlation of the expression of Glucose Regulated Protein-78 (GRP78) and the resistance to anticancer drug VP-16 in lung cancer squamous carcinoma cell line SK-MES-1, researched by Siyan et al.[32] Chemotherapy is hindered by cells that are resistant to the treatment. Little is known about the function of GRP78 because many in vitro detection methods are tedious, use large quantities of reagents, and require troublesome liquid handling procedures. The microfluidic chip contains an upstream concentration gradient generator and a downstream cell culture module. Their design was based on previous work by Jeon et al.[33] More will be discussed about cancer modeling on a chip in a later section.

A chip modeling the nasal passage, specifically the nasal epithelium, was designed by Wang et al.[34] This is useful because the nasal epithelial can be one of the first cells exposed to environmental agents. Human nasal cilia beating behaviors, a defense mechanism of the airway, were investigated by testing its reaction to gaseous formaldehyde. A microfluidic system was used because it allows for good control and offers highly sensitive molecule detection. The microchip was made from molded PDMS and contained a square chamber (10 mm × 10 mm × 30 µm, width × length × depth) separating two straight channels. Human nasal epithelial step progenitor cells (hNESPCs) were cultured on the device's membrane located at the square chamber. A bottle containing formaldehyde was connected to one of the straight channels (inlet), while a withdrawing syringe pump system was connected to the outlet. Cilia beating frequency (CBF) was monitored at different gaseous formaldehyde concentrations (0.5 mg m^{-3}, 1.0 mg m^{-3}, 3.0 mg m^{-3}). While the 0.5 mg m^{-3} trial remained relatively stagnant, the 1.0 mg m^{-3} trial showed a CBF that increased immediately and continued to increase throughout the course of the trial. When exposed to high concentrations of 3.0 mg m^{-3} formaldehyde, it was observed that CBF slightly decreased instead of increasing. This may be due to the toxic effects on the epithelial cells. The resulting experiment was shown to be a successful model of the nasal epithelium and has the potential to be used in clinical applications as well.

2.3. Intestine

Most oral drugs and nutritive substances are effective only after they are absorbed into the blood circulation through the intestine.[35] The evaluation of the intestinal absorption is important in the pharmaceutical and nutritional fields. The development of in vitro cell-based models for the intestine that mimic the mechanical, structural, and pathophysiological properties of drugs and nutrients is needed.

Organ–organ and drug–drug interactions are very important when working with drugs. How one cell reacts to another based on the effects of a certain drug can either allow a new drug onto the market or not. For example, van Midwoud et al.[22]

was one of the first to connect a liver and intestinal organ to allow for inter-organ interactions with applications towards toxicity testing. Bricks et al.[23] did a similar project using liver and intestinal cells as well.

A similar project that combined the liver with the intestine was done by Mahler et al.,[36] who used a microscale microfluidic cell culture analog (μCCA) of the gastrointestinal tract (GI), as well as the liver, to predict drug toxicity. APAP was used as a model drug to test the group's hypothesis that the passage and metabolism of APAP in the intestinal epithelial monolayer, followed by absorption into liver, would lead to low concentrations of glutathione and low viability of cells. Their goal was to create a complete in vitro human gastrointestinal tract model that is inexpensive, quick, and accurate to that of the human organs' response to orally ingested drugs, chemicals, and the resulting cell-cell interactions. In vivo, the lining of the small intestine membrane is composed of enterocyte and goblet cells. The enterocytes make up most of the population and control the transport of molecules, while the goblet cells secrete a mucus designed to protect the lining of the membrane. The functions of these two cell types must be taken into consideration in order to produce a working drug absorption model in vitro. The cell line Hepg2/C3A was used to represent the liver, while a co-culture of Caco-2 and HT29-MTX cell lines at a 3:1 ratio was used to represent the intestinal cells. The design consisted of a GI tract μCCA that led into a systemic μCCA that represented the liver, fat, kidney, and bone marrow. A peristaltic pump was used to control circulation and a reservoir compartment was connected to this system to control any sort of excessive pooling. It is important to note that only the GI tract and the liver pathways contained cells. The fat, kidney, and bone marrow chambers were only used to represent the distribution of fluid. The membrane was made of a polycarbonate with 0.4 μm pores and a Type I collagen coating. The cells were stained with calcein and monochlorobimane to visualize the monolayer integrity. Trials in this system were run for a course of 24 h. The results showed an inverse relationship between the concentration of APAP and the concentration of glutathione and cell viability. The products of APAP, APAP-GLUC and APAP-SULF, were monitored throughout the trials as well. Results showed that APAP-GLUC was produced fairly quick at the beginning of the experiment, but remained constant after the sixth hour. APAP-SULF showed concentrations that were ten times higher than that of APAP-GLUC for the first six hours, with a steady increase throughout the entire trial. This experiment showed GI tract-liver characteristics that showed they were able to digest APAP, with close observation to their viability and the products formed in the reaction. While they still are not able to produce the same levels of digestion as an in vivo equivalent, these results are fairly agreeable with in vivo results.

There have been many studies on the microfluidic in vitro design of the gastrointestinal tract and stomach for toxicity testing, drug testing, and mimicking key functional and structural parts. The use of hydrogels as a platform for cultivated cells in a GI tract design has been explored as well.[37] Sung et al.[38] developed a 3D collagen scaffold that mimicked the human intestinal villi. The technique used to create the hydrogel involved laser ablation to carve out holds on a plastic mold. This plastic mold was used to create a reverse-mold out of PDMS. Then, the reverse-mold PDMS was used to create a second mold that was made of calcium alginate. The hydrogel was built off of this mold, which eventually dissolved. The molds and structures were built with dimensions mimicking that of intestinal villi. Caco-2 cells were cultivated on the hydrogel villi, resulting in an in vitro system with close structural similarities to human jejunal villi. Cells could either be encapsulated in the hydrogel or seeded into the structure to be cultured. Collagen and polyethylene glycol diacrylate (PEG-DA) were used as the two types of hydrogels. Their system is simple and does not require expensive or complex equipment, which is a requirement for most microfabrication methods. While a microfluidic analysis was not done on the hydrogels, observation of the culture within the hydrogels revealed a successful layer of Caco-2 cells. With an analysis of flow from both sides of the device, a study of the dynamics of drug absorption in the GI tract can one day be done.

Although some models are used for the testing of toxins or drugs, a model for bacteria is rarely seen in microfluidic models. Kim et al.[39] created a model that had bacteria grown and added to healthy intestinal cells to see how they reacted. Instead of modeling the gastrointestinal tract for its functions and mechanical properties like with previous researchers, a GI tract infection was chosen as the focus. The system mimics the sequence of events in a gastrointestinal (GI) tract infection, specifically the invasion of bacteria on the intestinal cells. In the human body, a healthy GI tract can be defined by the balance of the interactions between the commensal bacteria and the intestinal epithelial cells. Pathogens often out-compete the bacteria and attach to the epithelial cells and begin an infection even though there are more commensal bacteria than pathogens. The molecular signals that are given off by the GI tract allow the commensal bacteria to prevent pathogen colonization or infection. In the model, this relationship is studied with a microfluidic device contained a co-culture of epithelial cells and bacteria. The group used E. coli as the prototypic commensal bacterium and HeLa S3 cells as the model for the intestinal epithelial cells. The pathogen used was E. coli O157:H7, a harmful strain of E. coli. The device consisted of a large chamber used to culture the epithelial cells and two "islands" used to culture bacteria. The two islands were located 1000 μm apart and were lowered and raised on a 100 μm thick PDMS wall. The cells grew a confluent layer and the bacteria produced a biofilm. Then the pathogen was introduced to the biofilm, followed by exposure of the epithelial cells. Resulting data showed a specific signal, indole, as having a huge effect on the resulting HeLa cell viability (which is directly correlated with the level of infection from the pathogen). Commensal bacteria that lacked this signal produced half the viability than when it was present. A trial in which 500 μM of indole was directly introduced to the pathogens also showed an increase in HeLa viability, but not to the extent of a natural signal. The group states that future work in determining biofilm thickness and the extent of the pathogen colonization are the next steps needed to better reproducing their model.

In 2012, the group of researchers from Kim et al. [40] developed a "human-gut-on-a-chip" that utilizes dynamic motions on the microdevice to better mimic the structure and function

ADVANCED
HEALTHCARE
MATERIALS
www.advhealthmat.de

Materials
Views
www.MaterialsViews.com

REVIEW

of the living intestine. This dynamic environment is created by the flow of the fluid through the channels, as well as the application of cyclic strain by use of vacuums within side chambers to mimic peristaltic motion. The design is similar to that of Huh et al. "lung-on-a-chip" design [7], in which two side chambers are utilized as vacuums to control the motions that the organ experiences in vivo (**Figure 5**A–C). This time, these distortions are used to represent the peristaltic motion experienced by the intestines (Figure 5D,E). The upper and lower microchannels are 150 µm high × 1000 µm wide, and are separated by a 30 µm thick PDMS membrane that has 10 µm pore size. Caco-2 cells were used to represent the intestinal epithelial cells, and were cultured on a PDMS membrane coated with ECM. Trials consisted of a Transwell plate for control and the microfluidic device containing just fluid flow, just mechanical distortion, and both. Results showed faster and higher quality Caco-2 cells in the trials using the microfluidic device. In the absence of fluid flow, the cells in the microfluidic trial resembled those in the Transwell plate. Additionally, the trial containing both fluid flow and mechanical distortion grew cells containing folds that resembled intestinal villi. To simulate the GI tract more accurately, cells obtained from a strain of *Lactobacillus rhamnosus*

GG (LGG) were used to simulate the microbes native to the intestines. The co-culture displayed greater integrity than the Caco-2 monolayer in the prior trials when exposed to fluid flow and mechanical distortion on the microfluidic chip. Therefore, this design was a success in introducing two variables to a gut-on-a-chip model: the integration of microbial cells native to the intestines and the dynamic motions inherent in the organ. Kim has explored these ideas further in other research papers.[41]

In contrast to Kim et al., the experiment done by Kimura et al.[42] used polarized Caco-2 intestinal cells in their microfluidic system. Polarized cells are known to mimic human organs, especially the human intestine, with much better accuracy. The developed microfluidic system was able to have long-term perfusion within the cell culture, as well as integrated optical fiber inserts used for fluorescent measurements within the device. The device contained two PDMS layers separated by a semipermeable membrane coated with collagen. A micropump controlled by a stir-bar was used to induce circulation of the medium. Once again Caco-2 cells were used to represent the intestinal cells and were cultivated on the apical side of the membrane. On the ninth day of cultivation, a confluent monolayer of cells was observed over the membrane. The cells
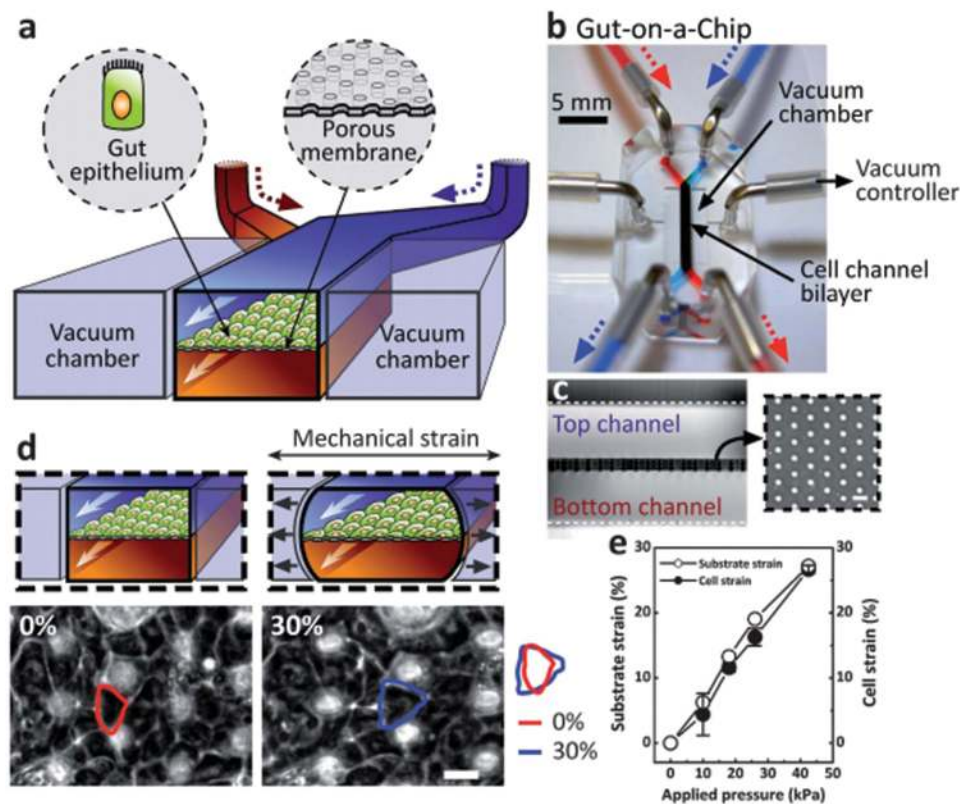

Figure 5. Layout for Gut-on-a-chip, with a) two co-current microchannels containing a membrane with cultured gut epithelium. Two vacuum chambers are located on either side of the device. B) An aerial view is shown of the actual device. C) A cross-sectional view is shown, with an aerial view of the membrane. D) When the vacuum chambers are active, mechanical strain is exerted on the device (upper two images). Cells showed that they would deform due to mechanical strain. The image on the bottom left circled in red is an epithelium cell before strain and the image on the bottom right circled in blue is an epithelium cell after strain. Note the image to the right showing an overlap image of the two, with the deformed cell clearing showing a larger width. E) Graphical results of the strain of both the substrate and the cells as a function of the applied pressure of the vacuums. Reproduced with permission.[40] Copyright 2012, The Royal Society of Chemistry.

www.MaterialsViews.com

ADVANCED
HEALTHCARE
MATERIALS

www.advhealthmat.de

REVIEW

were able to be cultured for up to 30 days and formed a tight monolayer. Transportation qualities were recorded by introducing rhodamine 123 into the medium, along with fluorescent beads, and recording the effects through the optical fibers. The results showed flow capable of long-term perfusion within the system. The functionality of the device and the measurements found through the results of the rhodamine 123 show that this has the potential to be a useful platform for drug screening as well as toxicity testing.

Some microfluidic systems are complex or have operating parts that not everyone can use. For this reason, it is important to think about simpler designs for microfluidic systems. Imura et al.[43] developed a microchip-based system that mimicked the human intestine. They had a microfluidic system to evaluate the intestinal absorption, with less cells and samples used and a shorter testing time. The design of the system was a two-tiered microchannel separated by a monolayer of Caco-2 cells that are cultured on a permeable membrane. The device had two PDMS sheets, each with its own microchannels that were 1.5 mm in width and 200 μm in height. The channels connected the upper and lower side of the PDMS sheets together. The upper channel worked as a microchamber for the cell culture. The membrane was made of a polyethylene terephthalate sheet that had 1μm sized pores and was coated with type I fibrillar collagen. Permeation tests were done to test the drug permeability of cyclophosphamide (CPA), using Lucifer yellow as a fluorescent marker. They also set bubble traps in the injection ports to prevent incursion into the chip. Since past structures had leaked the Lucifer yellow to the lower channel because of loose PDMS sealing, a new design was made. In this new design, the lower PDMS sheet and the membrane were tightly bonded to avoid leakage onto the other channels. Due to the cells becoming damaged because of unstable medium flow, the group cultured the cells statically and the medium was replaced on a daily basis. The Caco-2 cells formed a confluent cell sheet, and the Lucifer yellow could not permeate the membrane, while the CPA did. Good results were obtained with a lower flow rate; however, it also proved to be very time consuming. The Caco-2 cells reached confluence after 3 days and then remained this way for 10 days in the microchamber. When compared to conventional in vitro experiments, this system had practical characteristics of intestinal absorption.

Drug testing is one of the most important factors in intestinal microfluidic applications. Although many groups have used drugs for testing, none of them have used an array of drugs to study the effects they have in relation to each other. Yeon et al.[44] developed a microfluidic device to test drug permeability in the intestinal epithelial cell membrane. Researchers looked at 10 different drugs in order to test their permeability and compare the results with in vivo permeabilities. Instead of a membrane, the device trapped Caco-2 cells in microholes and measured the permeability of the drugs from there. The microfluidic device consisted of channels, each with an inlet and outlet, and a microhole array separating the two channels, and a channel for mixing. The microholes are 3 μm in diameter, 5 μm in height, and 30 μm in length. The microchannel height was 25 μm and most animal cells with a diameter of 5–15 μm could be trapped. The Caco-2 cells are imported into only one of the inlets, while a buffer is imported

through the other. Different flow rates from the two channels created a pressure difference that trapped the cells once they reached the microhole array. Once this occurs, the drug intended for testing is imported through the inlet originally containing the buffer. The drugs are absorbed by the cells in their channel, and travel through the mixing channel and into the outlet. The 10 drugs that were used for the experiment were: propranolol, naproxen, furosemide, antipyrine, verapamil, atenolol, piroxicam, hydrochlorothiazide, cimetidine and carbamazepine. The P_{eff} values that were measured in the microfluidic device were not the same as in vivo; however, they were still highly correlated with the permeabilities in the human intestine. This system reduces the assay time due to a non-complex system, and because there is no cellular membrane. The results found here has the potential to be used in predicting actual human permeability values of drugs, as well as a tool for drug discovery and toxicity testing.

2.4. Kidney

The renal transporters are located in the apical and basolateral membranes of the tubular epithelial cells. The effect of fluid shear stress on the cells is less understood than other major cells.[45] The renal epithelial cells experience mechanical forces due to variations in the urinary flow rate.

With toxicity being a main interest in the drug testing field, the kidney has been an organ of increasing interest for such tests. The kidney is exposed to fluid shear stress and it acts as a filtration system for the blood, as well as a vessel for the removal of toxins. The kidney transfers the toxins to the bladder, where they are then removed from the body during urination. Recall that Shintu et al.[20] used the liver and kidney, as well as cell co-cultures, to study their metabolic responses to various toxins. However, this section will focus on research done solely on the kidney.[46] One of those is Baudoin et al.,[47] who developed a microfluidic microchip that contained functional living cell microchambers that allowed for continuous cell feeding and waste removal. Their experiment consisted of a Madin Darby Canine Kidney (MDCK) cell culture on a PDMS-based cellular microchip that can be used for in vitro renal applications. Additionally, a toxicity study was performed on the microchip for the demonstration of large-scale toxicity applications. The group coated the PDMS chip in Fibronectin (extracellular matrix protein). The first PDMS layer with the microstructures contained a series of 300 μm × 300 μm × 100 μm microchambers and 400 μm × 150 μm × 100 μm microchannels, which were all contained inside a cell culture chamber. The second layer of PDMS was used to close this cell culture chamber. Culture media was brought into the microchip system through a culture medium tank, and the flow was induced through a peristaltic pump. These devices were formed as a circuit, thereby creating a perfusion loop. For toxicity tests, ammonium chloride was used. The initial experiments tested the viability of cells in the system as it ran inside a CO_2 incubator for various flow rates (0, 10, 25, and 50 μL min^{-1}). The results showed it was able to run while keeping a viability above 90% for almost all flow rates, except for at 50 μL min^{-1}. At 50 μL min^{-1}, the cell detached from the surface after a 24 h

ADVANCED
HEALTHCARE
MATERIALS

www.advhealthmat.de

Materials
Views
www.MaterialsViews.com

REVIEW

perfusion and viability was found to be below that of 10%. Cell density tests showed that at static conditions, the number of cells stayed roughly the same, regardless of their initial count. At flow conditions, slight proliferation of cells was observed at flows of 10 μL min^{-1} and 25 μL min^{-1}. The addition of ammonium chloride as a toxicity agent caused the reduction of cell proliferation. This reduction was most prevalent in the 10 μL min^{-1} trial. The addition of ammonium chloride also led to an increase in the consumption of glucose and a decrease in the production of ammonia.

The integration of fluid shear stress is an important factor that can increase the relevance of an in vitro model. Jang et al.[48] developed a multi-layer microfluidic device that utilizes fluidic shear stress for a more complete renal model. They used primary rat inner medullary collecting duct (IMCD) cells as their model to be cultured inside the microfluidic channel. A fluidic shear stress was applied to the device to generate a realistic environment for the cells. The device consisted of two layers of PDMS, with a polyester porous membrane between them. The bottom layer of PDMS was used as a reservoir, while the top layer contained a microfluidic channel that would be used for fluid flow. After 3 days of culture, the cells were brought into the system and a fluid shear stress was applied for 5 hours using a syringe pump. After the shear stress was applied, 1 mm of hydrogen peroxide solution was added to the fluid regions to test the cell viability. Hydrogen peroxide was also added to a control culture that was cultivated on a glass surface separate of the device. The results showed that after 2 hours of treatment, the device under fluid shear stress already displayed a significantly higher viability than the glass control. Additionally, the system showed accurate cell separation associated with its cell polarization. Molecular transport was also analyzed by applying vasopressin and aldosterone into the lower PDMS reservoir to induce hormonal stimulations into the system. Vasopressin is able to induce water transport, while aldosterone induces NA transport. Both of these results agree with in vivo expectations. This system can be used as a model for diseases like diabetes or edema, as well as a model for studying renal physiology.

In the year 2010, Jang studied the kidney cells and showed the polarization and transport of the primary rat inner medullary collecting duct (IMCD) cells as well as the application of fluid shear stress (FSS). Now in the year 2011, Jang et al.,[49] developed a "collecting-duct-on-a-chip" to further investigate the effects of changes within a renal environment. The role of the collecting duct in the kidney is mainly to maintain homeostasis of fluids through transportation across its membrane. Specifically, the role of the protein aquaporin-2 (AQP2) was observed under these altered conditions due to the major role it serves in water transport across the membrane. Additionally, the role of the actin cytoskeleton present in in vivo collecting ducts (F-actin) is explored in the model. Like their previous design, the main components that made up the chip consisted of a PDMS reservoir and a PDMS layer complete with microchannels for active fluid flow, as well as a polyester membrane separating them. Fluid shear stress, hormonal stimulation, and an osmotic gradient across the membrane will serve as the active changes within the system. Fluid shear stress at 1 dyn/cm^2 and arginine vasopressin stimulation (AVP) were applied in

the microfluidic chip for trials consisting of F-actin within the IMCD cells. A strong fiber network was observed roughly 1 hour after the start of the trial, with a slow depolymerization occurring up until hour 5, when the F-actin was fully depolymerized. It was also observed that if system was left undisturbed after depolymerization, the F-actin would repolymerize after roughly 2 h. Additionally, the application of an osmotic gradient was shown to lead to a full F-actin depolymerization. This system can be used as a tool for drug screening of the regulation of AQP2 as well as being an important model for fluid homeostasis.

Most recently, Jang et al.[50] made a microfluidic device that mimicked the functions of the human proximal tubule using primary human kidney epithelial cells. Although they only used one type of cell, their research brings forth more information that is needed to help the problem of accurate drug development. Their system, just like others, can be used to replace two dimensional cell culturing and animal testing for the ability to test for toxins in organs. The device shows many similarities to their previous design.[49] Once again, the main components consisted of a lower reservoir and an upper microfluidic channel with a porous membrane containing ECM collagen separating the two. The cells were cultivated on the porous membrane, in which well-defined monolayers were observed after 3 days for both static and fluid conditions. The addition of fluid shear stress created an even more realistic cell layout, with a system of cell columns consistent with their in vivo cell polarity (**Figure 6**). Analysis of the system showed that the levels of albumin uptake, expression of brush-border alkaline phosphatase, and glucose transport were greatly increased when flow was introduced into the system. To observe toxicity effects, the cells were treated with cisplatin for 1 day and then were allowed to recover by keeping them drug free for 4 days. The magnitude of recovery was significantly higher in the system containing flow. The use of primary human kidney epithelial cells, along with a model used in static and dynamic conditions, presents a method that shows promise for renal toxicity analysis.

Since fluid shear stress is very important in the function of the kidneys, Frohlich et al.[51] developed a microscale tissue modeling device (MTMD) to represent an accurate renal system. This device focuses on utilizing fluid shear stress and a topographical pattern to mimic its in vivo counterpart. The device consisted of a lower silicon plate that contained sub-micrometer topographical features such as grooves and pitches, and an upper PDMS layer containing a microfluidic path. The human renal proximal tubule cell line HK-2 was chosen to represent the tissue. The HK-2 cells were stained with ZO-1 fluorescence to analyze the tight junction formation. Blank substrates in the presence of FSS showed a much lower ZO-1 intensity and a more disorderly array of cell structure. Topographic substrates without FSS showed a higher ZO-1 intensity and a better array of the cell layer. In the presence of both, the cells showed a well-defined tight junction with good intensity. Therefore, while FSS seems to play a bigger role in the modeling of the kidney, a combination of both yields the best results.

The role F-actin plays in the transportation of nutrients across the membrane was also analyzed by Ferrell et al.,[52] who used electrodes designed to take TEER measurements to
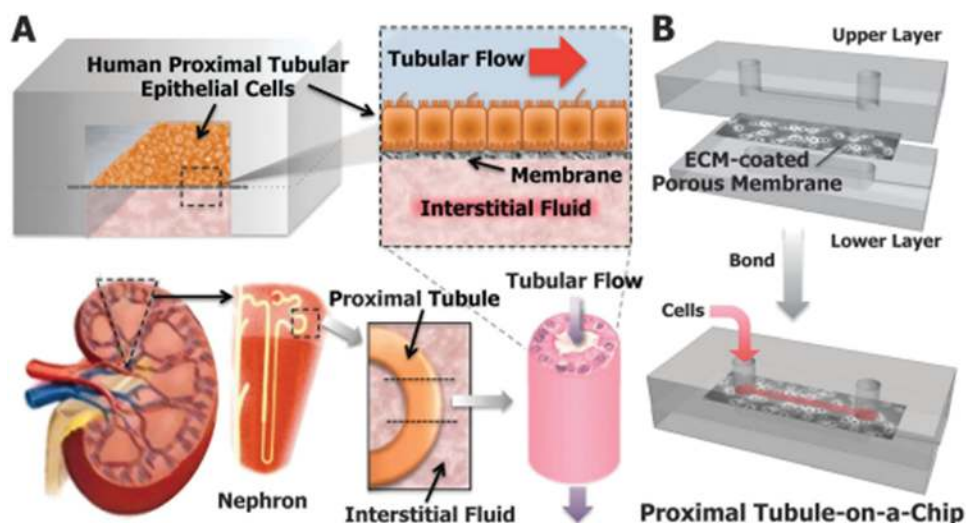
Materials
Views
www.MaterialsViews.com

ADVANCED
HEALTHCARE
MATERIALS
www.advhealthmat.de

REVIEW

Figure 6. Design layout for the device, showing A) a cross-sectional view. The device mimics the human proximal tubule of the kidney (pictured below). Human proximal tubuluar epithelial cells are cultivated on top of the membrane, with tubular flow occurring on the apical section, and interstitial fluid located on the basolateral section. B) The device shown layer-by-layer. Two design consists of an upper layer containing a microfluidic channel and a lower layer containing a fluid reservoir. Reproduced with permission.[50] Copyright 2013, The Royal Society of Chemistry.

analyze a working kidney bioreactor under fluid shear stress conditions. TEER measurements have shown to provide excellent inside into the tight junction permeability properties of a cell culture. Additionally, transportation properties were analyzed, with special focus on the structure of tight junctions (ZO-1) and cilia formation (acetylated α-tubulin) within the cells, and the F-actin cytoskeleton array that facilitates transfer. The device consisted of an apical chamber complete with 8 microfluidic channels and a basolateral chamber used as a reservoir. An array of 200 µm diameter posts was used to support the membrane on the bottom chamber and allow fluid transport. A polycarbonate membrane was connected to separate the two chambers. A perfusion circuit was created, consisting of the bioreactor, a perfusion pump, and a medium reservoir, all connected through silicone tubing. For TEER analysis, electrodes were inserted within the tubing, with the ends exposed within the bioreactor. Additionally, all trials were conducted within an incubator. A shear stress of 1 dyn cm^{-2} was used for fluid shear stress trials. Both human renal epithelial cells (HREC) and MDCK cells were cultivated on the membrane. Initial culturing results showed that the MDCK cells were able to form a monolayer within 3–5 days, while the HREC cells took 10 days. Staining techniques were used to analyze the formation of tight junction proteins, cilia, and F-actin (HREC only). Both ZO-1 proteins and acetylated α-tubulin were observed in the

model, showing well-defined borders and distinct formations (**Figure 7**a,b). Additionally, the role of F-actin in static conditions showed a normal layout of F-actin (Figure 7c), while fluid
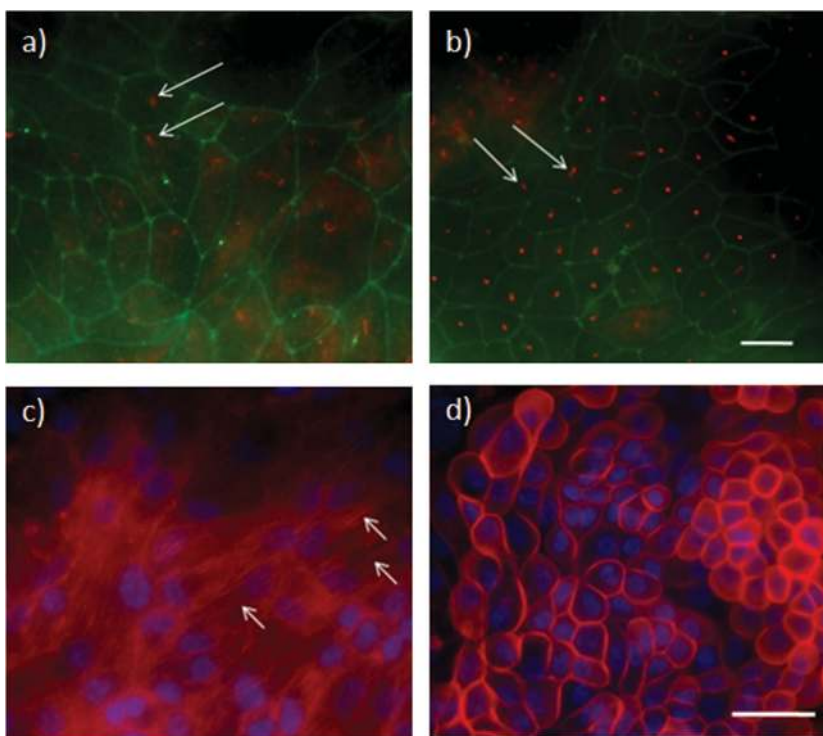

Figure 7. Immunofluorescence staining results depicting the formation of a) MDCK monolayer and b) HREC monolayer, each containing well-defined tight junctions (green outline) and primary cilia (red dots addressed by arrows). Additionally, HREC was stained for F-actin analysis under c) static conditions and d) fluid shear stress conditions. Arrows in (c) indicate F-actin fibers. Scale bars in (b) and (d) are at 25 µm. Reproduced with permission.[52] Copyright 2010, Wiley.

ADVANCED
HEALTHCARE
MATERIALS
www.advhealthmat.de

Materials
Views
www.MaterialsViews.com

REVIEW

shear stress conditions showed the F-actin surrounding the cell (Figure 7d). It is believed that this is a normal response of the cytoskeleton to shear stress and is similar to what happens in the cells of humans. The system was then monitored with the addition of Ca^{2+} into the medium, which is known to have a positive effect on the structure of tight junctions. A switch technique was used to measure transient changes, where the system would switch between using a medium containing normal levels of Ca^{2+} to low levels of Ca^{2+}. After analysis, normal levels of Ca^{2+} were restored and the system was allowed to recover. The switch from normal to low levels of Ca^{2+} showed a TEER that contained 45% of its original resistance. Using inulin as a marker, the results showed a large increase in leakage rate when the switch to low Ca^{2+} levels was made (from 0.09 ± 0.03 µg cm^{-2} min^{-1} to 0.39 ± 0.09 µg cm^{-2} min^{-1}), showing the potential breakdowns of cell interactions when transient changes are applied.

Analysis of mass transfer has also yielded results.[53] Ramello et al.[54] investigated the properties of mass transfer in a microfluidic kidney model. They also analyzed the transportation by using different drugs. The study used MDCK cells on a polyethersulfone (PES) membrane inside a PDMS chip. The chip contains an upper and lower chamber, each containing an inlet, outlet, peristaltic pump, and filtration chamber in co-current circulation. This was done to create a system in which one chamber contains a reservoir of filtrate while the other contains retentate. The retentate circulation would initially contain the molecule used for inspection, while the filtrate circulation would capture the filtered molecule. Molecules used for this experiment were chosen based on their variety in size. Caffeine was used as a small marker, vitamin B12 was used as a medium marker, and albumin was used as a large marker. The value of cell membrane permeability before mass transfer studies was measured as being equal to 1.8 ± 0.2 mL min^{-1} cm^{-2} bar^{-1}, and the value without cells was 9 ± 3 mL min^{-1} cm^{-2} bar^{-1}. Trials involving mass transfer were compared with mathematical models, with cells and without cells on the membrane. The results showed an inverse relationship with molecular weight; there was a notable increase in mass transfer as the molecular weight decreased. Mass transfer through a membrane without cells yielded higher rates of mass transfer for all trials. When treating the cells as a separate diffusive layer, the mathematical models fit the experiment results perfectly. In an attempt to model toxicity in the system, acrolein was used at varying concentrations. For each molecule tested, there appeared to be a threshold in which acrolein did not play a factor in the mass transfer of the system. The larger the molecular weight, the higher the threshold. Above this threshold, the diffusive coefficient was found to be higher than trials without acrolein. A second threshold was observed, in which surpassing it yielded a time-dependent mass transfer rate. The permeability of the membrane was measured after the acrolein trials, which revealed an increased permeability of 8 mL min^{-1} cm^{-2} bar^{-1}. Thus, these experiments showed the effects of molecular weight and toxicity on the permeability and mass transport properties of the system. These results agreed with past research and mathematical models and have shown that they can be a useful model for modeling mass transport on a renal biochip.

2.5. Heart

The function and development of the heart mainly depends on the response of the cardiac cells and the mechanical stress. In order to have new successful drugs and medicine, it is important to understand the biological functions of the heart. Current cell culture systems fail to accurately represent the physical, mechanical, and biological functions of the heart. There have been studies that have tried to model the heart; however, most are two dimensional, and although they do show some mechanical properties, they are not the best for accurately mimicking the human heart as they do not have complete heart properties and do not allow for fluid flow or similar work.[55] For this reason, three dimensional microfluidic systems for the heart are being explored as well.

Many groups have designed various systems to model the human heart and to mimic the key mechanical functions and properties.[56] Due to the advantages of 3D microfluidic systems, there has been a shift towards using these designs to represent cardiac situations.[57] Giridharan et al.[58] developed a model designed to replicate physical loading in the left ventricle. This microfluidic cardiac cell culture model (µCCCM) contains a cell culture chamber, a pump, a collapsible pulsatile valve, and an adjustable hemostatic valve. The cell culture chamber consists of a PDMS membrane between two polycarbonate plates, milled with microfluidic channels to create perfusion through the membrane. The embryonic cardiomyoblast cell line H9C2 was used for cultivation on the membrane. The pump serves the purpose of supplying flow, and therefore shear stress and fluid transport, to the system. The pulsatile valve is used to produce mechanical stress into the system in the form of pressure build-up in the cell culture chamber, resulting in the stretching of the membrane. A closed valve builds pressure while an open valve relieves pressure, thereby being capable of representing cardiac preloading. The hemostatic valve is used to control flow resistance, and is a representation of afterloading. These devices are connected as a circuit to provide circulating fluid flow. This device was first tested by applying different levels of pressure for a variety of membrane thicknesses. The strain was found to be inversely proportional to membrane thickness, displaying a 20% strain for a 139 µm thick membrane and 60% for a 93 µm thick membrane. Next, the device was characterized for normal conditions, as well as for abnormal conditions such as: heart failure, hypertension, hypotension, tachycardia, and bradycardia. The simulation of cardiac disorders was done through the programmable valves connected to the system. Values obtain from these trials depict fairly comparable results with their in vivo counterpart. When comparing the cellular make-up between static trials and the trials within the µCCCM, results showed that the static culture make-up resembled fibroblasts, with randomized F-actin, while the µCCCM displayed a rectangular, boxy make-up with aligned F-actin. This shows the capabilities inherit in modern microfluidic cardiac models, especially when considering abnormal heard conditions.

When dealing with in vitro microdevices for tissue engineering or drug delivery[59], external power sources are depended upon to supply energy into the system. However, if the device requires implantation into an in vivo source, external
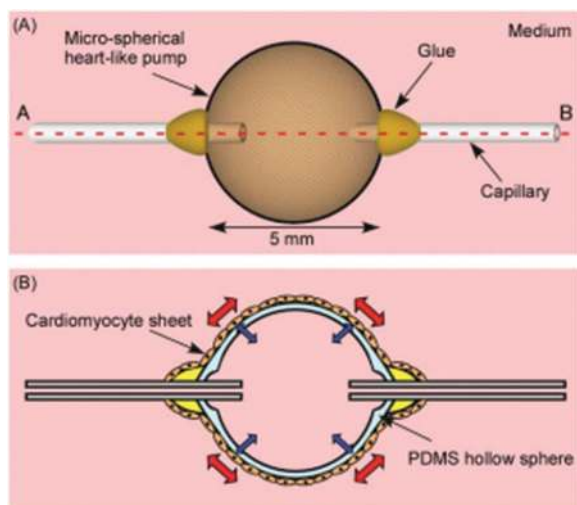
www.MaterialsViews.com

ADVANCED
HEALTHCARE
MATERIALS
www.advhealthmat.de

REVIEW

Figure 8. Diagram of the micro spherical heart pump, shown in A) a full view, diplaying the components of the device and medium brought in through port A and expelled through port B. Additionally, B) a cross-sectional view is shown. The layer containing the rat cardiomyocytes can be seen, with red arrows shown to display their contracting nature on top of the PDMS sphere. Reproduced with permission.[60] Copyright 2007, The Royal Society of Chemistry.

power sources must be eliminated. Tanaka et al.[60] fabricated a micro spherical pump made from cardiomyocytes to represent the heart functions. The hollow sphere was created by inserting a capillary tube through the entirety of a sugar ball, so that both ends of the capillary could be observed outside of the ball. A layer of PDMS was applied around the sugar ball, and the capillary tube was pulled back to allow a second capillary tube to connect to the other side, and both tubes were glued into place. A pump was applied through one of the capillary and water was introduced to dissolve the sugar. This resulted in a hollow sphere with a thickness of 250 μm (**Figure 8**a). Rat cardiomyocyte cells were cultured and placed on the surface of the PDMS sphere. Spontaneous pulsating was observed within one hour of incubation, which eventually became periodic beating (Figure 8b). Fluoro Sphere particles were introduced into the medium for tracking. The results were determined with a particle displacement data set which estimated the parameters for the performance of the fluid bio-actuation. The following equation was used to describe the change in microchannel volume as a function of the change in chamber volume:

$$\Delta v = 1/2 \Delta V \tag{2}$$

where Δv is the volume change in the microchannel and ΔV is the volume change in the chamber. Using $\Delta v = 0.5\ x\pi r^2$ as an approximation due to its circular cross-section, where x is the displacement of particles near the capillary center and r is the inside radius of the capillary, ΔV was found to be 2.2 nL. From there, the following equation was used:

$$Q = f\Delta V \tag{3}$$

where Q is the flow rate and f is the beat frequency. They found that f was 0.6 Hz at 37 °C, which resulted in a final

Q value of 0.047 μL min⁻¹. Long-term trials showed that the device could be functional for up to 5 days. They compared it to other typical micro chemical systems and showed that it is possible to use the system Tanaka et al. made in micro chemical or biochemical applications. They confirmed that their device was flexible and biocompatible and very similar to other polymer pump actuators. They concluded that if their heart device functioned continuously for at least 5 days, the cells of cardiomyocytes that were inside the sphere would live for that amount of time as well. They stated that this can be used to mimic animal hearts; however, it is worth noting that there are multiple chamber valves and walls required for this process. To do this they used an in situ laser photo-fabrication technique. These results and their microspherical heart pump are very important as it is a step towards having electric powerless bio-actuators for fluids in implants and also for micro model cardiovascular circulatory systems for monitoring applications.

A different study to that done by Giridharan et al. and Tanaka et al. was done by Li et al.,[61] who fabricated a microfluidic chip that uses integrated acoustic wave sensors to analyze cardiomyocyte contraction. The sensor works by applying a voltage to the electrodes located on both sides of a flat quartz crystal plate. The voltage induces acoustic waves from the crystal due to the piezoelectric effect. These acoustic waves will be produced in the thickness-shear mode (TSM) and applied to the cardiomyocyte cells. Any change in stiffness will result in a modified resonant frequency. This method can be used to identify pulsating properties of the cells. The device consists of an upper glass plate milled with microfluidic channels and a bottom quartz crystal plate acting as the TSM sensor. Cells were fit into the channels of the glass plate. Data showed that the device without the channel plate was capable of reacting to changes in the system for all parameters. Changes in the system include additions of cell suspension and a bath solution. The parameters were shown to make corresponding changes at the intervals at which the changes in the system were applied. The experiment was then run using the channel plate. The results showed mixed results that only proved that the system wasn't fully capable of responding to the acoustic waves. The group believes that offsetting contractions may have been one of the underlying problems in the experiment, and therefore a shorter interval between data points may be able to rectify this problem.

While not falling into the classic mold of organ-on-a-chip systems, the method of testing extracting organ tissue instead of cultivating cells is another potential method for understanding organ function in vitro. Owaki et al.[62] proposed a microvascular connection method called the "suction-induced vascular fixation method" or SVF method. They were able to use tissue from an extracted chick heart and connect it to their microfluidic system. The SVF method consists of using a suction technique to bring all the blood vessels through a microfluidic device. This constrains the vessels so that they are easily manipulated and can be analyzed with less degrees of freedom. The microfluidic device consists of a PDMS layer containing holes designed for integration with the blood vessels of the chick heart, as well as a perfusion chamber to maintain functions of the organ. Due to the variability and uncertainty

of blood vessel diameters, the device allows several vessels through one hole if the vessels prove to have a smaller diameter than expected, and can also be rejected if the vessel diameter is too large. While the main goal of their experiment was to design an alternative method to handle the analysis of organ tissue, an addition test was done in which a solution was sent through the device and into the embryonic heart. The results showed that a periodic circulation could be achieved through this method, and the heart was able to periodic beat using this method.

2.6. Vasculature

Endothelial cells that line blood vessels are designed for functions such as: facilitating blood flow, enabling nutrient transfer through the vessel, and regulating surrounding tissue growth.[63] A viable microcirculation is required in in vitro models if we are to interconnect organs. This will be especially important if a "human-on-a-chip" design is created. However, this section will focus on a microfluidic model for isolated vasculature. It is vital to have a realistic in vitro model for drug development and the study of cell–cell interactions.

Research into 3D in vitro vasculature has produced a variety of results.[64] However, the design of functional artificial vasculatures has been a difficult hurdle to overcome. Borenstein et al.[65] have specifically addressed this issue in their design. The microchip design displayed one inlet and outlet, with a bifurcating microchannel network stemming from each end and joined such that the design showed a symmetric pattern. To better mimic human vasculature, all channels were designed with circular cross-sections, and each new generation of bifurcation had a smaller cross-sectional area than the last (**Figure 9**). The diameters chosen for each subsequent channel were based off of Murray's Law. Polystyrene was used as the material for the chip due to its stability and a better understanding of the surface properties. Two layers, each containing the network with cross-sectional channels, were created using an electroplating technique. Human umbilical vein endothelial cells (HUVEC) were cultivated on the inner surface of the channels. Results showed a stable and consistent monolayer throughout the channels. Thus, the goal of creating a microfluidic chip capable of accurately representing human vasculature proved successful. While flow was not examined in this experiment, the circula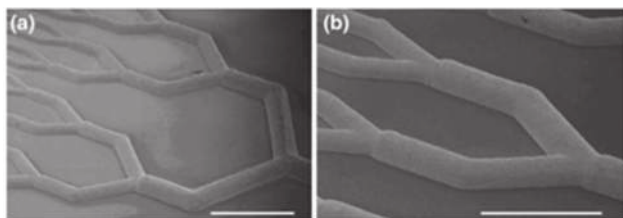r cross-sections and smooth transitions between bifurcations and diameter changes have potential for use in microfluidic vasculature chip designs.

In pursuit of a physiologically similar vasculature model, considerations such as multi-cell interaction and dynamic stress on the system should be considered. The design created by Srigunapalan et al.[66] looked at the effects of shear stress, monocyte-EC adhesion through TNF-α stimulation, and monocyte transmigration on a microfluidic vasculature system. The device consists of two PDMS layers, with the top layer displaying a straight microchannel and the bottom player displaying an S-shaped microchannel. A polyethylene membrane containing 8μm pores is used to separate the two layers. Circulation of flow was provided through a peristaltic pump that would take media from a reservoir compartment and feed it through a damper, followed by the microfluidic chip, then back into the reservoir, completing the cycle. The purpose of the damper was to force continuous flow (as opposed to pulsatile flow) into the chip. Porcine aortic endothelial cells (PAEC) were chosen for the EC and were cultivated on the top of the membrane. Initial trials tested this system under static and dynamic conditions, with dynamic conditions providing a shear stress of 20 dyn cm^{-2}. Results showed elongation of the PAEC for dynamic trials. Further trials introduced TNF-α stimulation into the culture, followed by monocytes (RAW264.7 cells) applied with fluorescent dye. Monocyte adhesion was tested as a function of both TNF-α stimulation and its static/dynamic state. Results showed that TNF-α was the biggest factor in monocyte adhesion, while the trials under fluid shear stress proved to have slightly better adhesion capabilities than their static counterparts. Trials done for testing transmigration used THP-1 cells for monocytes. THP-1 was introduced in the top channel and adhered to the PAEC. Transmigration effects were observed through the membrane as the monocytes travelled into the bottom channel. Stimulus effects were observed with the protein MCP-1, introduced solely in the bottom channel. Results from these trials showed that the introduction of MCP-1 lead to a roughly ten-fold increase in the number of transmigrated monocytes per square millimeter. Therefore, the effects of cell-cell interaction and stimuli replicated various scenarios in a microfluidic vasculature chip. The best conditions for in vitro monocyte adhesion are with TNF-α stimulation and fluid shear stress conditions, and the best conditions for transmigration are with MCP-1 stimulation. This shows how additional considerations within the device to mimic in vivo vasculature have the potential to produce the best results.

2.7. Other Organs

While the organs with the most prevalent research have been highlighted in previous sections, organ-on-a-chip systems have the potential to be used for many different organs. Researchers have been able to branch out in this respect and explore different ideas in unique systems tailored to their chosen organ. Additionally, microfluidic organ-on-a-chip systems with cancerous organs will be explored, as well as multi-organ chips aimed to produce results working towards a body-on-a-chip.

Figure 9. Image of the device. A network of bifurcating channels, each level containing a diameter smaller than the last, is shown. The scale bar is displayed at A) 1 mm and B) 500 μm. Reproduced with permission.[65] Copyright 2009, Springer.

2.7.1. Bone Marrow

Torisawa et al.[67] designed a working bone marrow-on-a-chip device to replicate in vivo functions and study the effects of radiation-induced toxicity. The design features a PDMS cylindrical ring containing demineralized bone powder (DBP) and bone morphogenetic protein 2 and 4 (BMP2, BMP4). A PDMS cap was placed over the top cavity of the ring to better regulate adipocytes for better hematopoiesis. Cultivation of these materials within the device was performed in vivo through implantation within a mouse. After 4–8 weeks, new bone structures were formed with a marrow inner region showing signs of cellular activity. The most prominent cells within the marrow were hematopoietic cells. Cultivation for 8 weeks within the mouse yielded the best results, with an array of cells that mimicked naturally grown bone marrow. Once the artificial bone marrow was removed from the rat, it was placed within a microfluidic PDMS chip (**Figure 10**a,b). This chip contained PDMS layers containing microchannels designed above and below it. Two porous membrane layers were positioned between the layers containing microchannels and the culture chamber. The device showed it was capable of maintaining its structure and function for up a week with a medium containing cytokines. In comparison with naturally grown bone marrow extracted and cultured in a static system, the results from the microfluidic system showed similar functionality and viability of long-term hematopoietic stem cells (HSC). Freshly isolated bone marrow from both systems displayed the highest number of long-term HSC, with each subsequent day showing a decrease in that value. Additionally, the naturally grown static trial also displayed a significant increase in progenitor cells after a period of time compared to freshly isolated bone marrow. Further trials exposed the microfluidic bone marrow device to γ-radiation to observe the toxic effects on the organs functionality and cell viability. For control purposes, a system of the previously mentioned static culture with naturally grown bone marrow, as well as live mice, were tested as well. The various cell viabilities were tested at different radiation dosages. The results showed an inverse

Figure 10. A) Process of obtaining bone marrow cells highlighting the several key steps: implanting the device containing bone-inducing materials within the mouse, letting it cultivate within the mouse for 8 weeks, and introducing the eBM (engineered bone marrow) into the chip. B) Images of this process can be seen, shown before implantation (left), after extraction from the mouse (middle), and the chip containing the eBM in its entirety. Scale bar is at 2 mm. Reproduced with permission.[67] Copyright 2014, Nature Publishing Group.

relationship between γ-radiation dosage and cell viability for the HSC, progenitors, lymphoids, and myeloids. Granulocyte colony-stimulating factor (G-CSF), shown to inhibit radiation effects and promote recover of bone marrow in mice, was also tested in this fashion. Results showed that G-CSF did indeed provide a higher cell viability for bone marrow cells. Thus, the system was able to provide in vitro bone marrow functionality under normal conditions and toxic conditions that are comparable to in vivo results. Future toxicity tests with bone marrow diseases have the potential to be utilized using this technique.

2.7.2. Brain

Delivery of drugs and nutrients into the brain is regulated by the blood-brain barrier (BBB). On the blood side of the barrier lies a complex array of vascular endothelial cells, and on the brain side lies the central nervous system. Issues maintaining functionality of the BBB can result in neurological disorders. Thus, it is important to understand and test the effects that drugs might have on the BBB through in vitro design. Therefore, with respect to the brain, most microfluidic models will feature a BBB-on-a-chip.[68] Griep et al.[69] designed a working BBB-on-a-chip and tested its functionality through TEER measurements. Two PDMS layers were constructed with a straight microfluidic channel that was positioned so that the top channel was perpendicular to the bottom channel. Additional grooves were created to fit in the electrodes for TEER measuring. A polycarbonate membrane was positioned between the two layers. Human brain endothelial cells (hCMEC/D3) were cultivated in the top channel and showed a confluent monolayer within 1 day. TEER results showed similar results between a static culture and the BBB chip, both displaying tight junctions and a confluent monolayer. Next, the effects of fluid shear stress on the hCMEC/D3 were tested. After 3 days of normal function in the device, the BBB chip was exposed to shear stress of 5.8 dyn cm^{-2} for 18 h. Results showed that the TEER value triple during the duration that shear stress was applied to the system. Afterwards, the effects of TNF-α stimulation was tested on the device. Directly following the 18 h of exposure to fluid shear stress, 1 ng mL^{-1} of TNF-α was introduced to the system for 2 h. Results showed that the TEER value dropped 10-fold when TNF-α was introduced. While this may show that the effects from TNF-α in the system make a much bigger impact than fluid shear stress, it is important to note that increasing TEER values is much more difficult to achieve than decreasing, since even the slighted gap in the cell monolayer can significantly reduce TEER values.[3a] This experiment shows the capabilities of BBB models, with research already capable of considering the biochemical and mechanical factors that may contribute to its function.
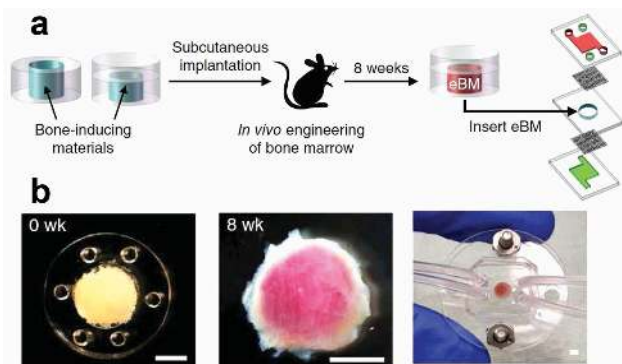
2.7.3. Spleen

In the human body, the spleen serves the role of filtering blood, recycling red blood cells, and containing a reserve of white blood cells. While a spleen can be removed from the body without suffering fatal injuries, it still serves important roles; of which an in vitro understanding can benefit, especially with an

REVIEW

ultimate goal of creating a "body-on-a-chip." A "splenon-on-a-chip" design was created by Rigat-Brugarolas et al.[70] This design mimics the red pulp area of the spleen by creating a fast-flow layer and a slow-flow layer. The fluid going through the slow-flow layer travels through a straight channel representing the 10% of blood that goes through a filtration process, where unhealthy red blood cells are destroyed. This channel also contains an area filled with a pillar matrix, thereby impeding the flow and increasing the density in that area, representing a reticular mesh observed in an in vivo spleen. The fluid going through the fast-flow layer travels in a zig-zag pattern representing the rest of the blood going through the bypass of the filtration process. This device is connected to a syringe pump, providing flow at 5 µl min^{-1}. Deformability studies can be performed on the device, with cells incapable of deforming showing constriction in the channels. Initial tests in the microfluidic system looked at the differences in deformability between new and aged red blood cells (RBC's). Results showed that ages RBCs showed less deformability than new RBCs. The infected red blood cell (iRBC), *Plasmodium yoelii*-GFP, was then tested and compared to healthy RBCs. The results showed that healthy RBCs had a deformation measurement of roughly 19%, whereas the unhealthy iRBCs had a deformation measurement of roughly 34%. This device shows a unique way of representing a 3D microfluidic spleen capable of identifying pathogens based on their deformability.

2.7.4. Cancer/Tumor

Modeling in vitro microfluidic chips to represent in vivo cancerous situations is a popular area of research. Models involving lung,[71] breast,[72] prostate,[73] pancreas,[74] brain,[75] cancer have been created. Song et al.[76] designed a microfluidic device to replicate the functionalities of breast cancer cells in a vasculature system. The design consists of two PDMS layers containing microchannels, and a polyester membrane positioned between the layers. The microchannel on the top layer contains a funnel-shaped inlet with a straight channel, while the bottom layer contains two straight channels located perpendicular to the top channel (**Figure 11**A, D). Human dermal microvascular endothelial cells (HDMEC) are cultivated on the top of the membrane (Figure 11C). Trials consisted of introducing chemokines (CXCL12) contained in the medium through the lower channels, with breast cancer cells (MDA-MB-231) circulating through the top channel, with a focus on the adherence of the cancer cells on the endothelial cells in the overlapping channels (Figure 11B, E, F). One of the contributing factors to
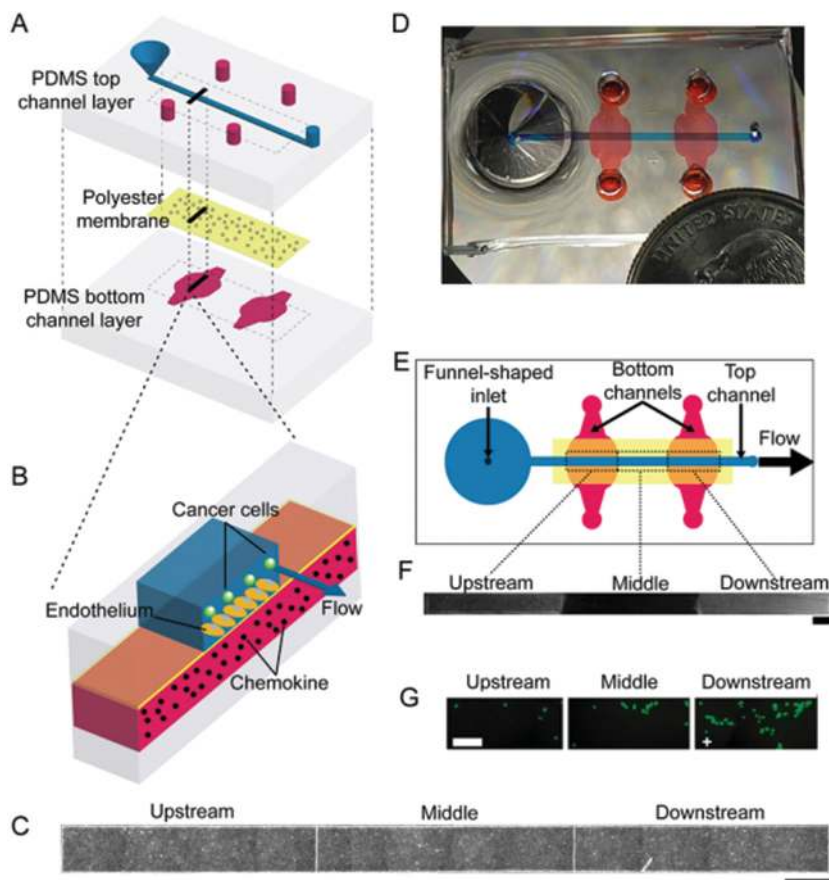

Figure 11. Design of the device, showing A) a layer-by-layer layout of the two PDMS layers with a membrane in-between them. B) A cross-sectional view of the device can be seen at the location where the channels overlap, showing the flow of medium with cultured cells. C) HDMEC cultivation shown by region (upstream, middle, downstream) through phase contrast imaging (scale bar at 800 µm). D) An actual photo of the device, with a quarter for scale. E) Aerial view of the device, showing the locations of overlap, as well as the direction of flow. F) Interaction of HDMEC cells with flow from lower channel can be seen through fluorescent staining. Fluorescent dye was administered in the lower channels, showing interaction with the sections overlying the bottom channels, but not in the middle (scale bar at 800 µm). G) Adhesion of MDA-MD-231, with TNF-α treated only at the downstream channel (scale bar at 200 µm). Reproduced with permission.[76] Copyright 2009, Public Library of Science.

cancer cell adhesion to the endothelial walls is the expressions of CXCR4 and CXCR7 receptors. Therefore, trials using cancer cells expressing CXCR4 (231-CXCR4) and CXCR7 (231-CXCR7) were also used to study their effects. Results showed that all three trials showed increased adhesion with faster flow rates. A significantly larger adhesive ability was also noted for trials containing CXCL12 in the HDMEC than trials without it. However, the ratio of treated cells to untreated cells showed similar values for all three. Therefore, while CXCL-12 enhances adhesion, it is independent of CXCR4 and CXCR7. To study the role HDMEC plays on adhesion, new trials were conducted in which the HDMEC monolayer was treated with CXCL12, which is known to up-regulate CXCR4, TNF-α, which is known to up-regulate both CXCR4 and CXCR7, and AMD3100 in combination with CXCL12, which inhibits binding for CXCL12-CXCR4, but not CXCL12-CXCR7. These were tested in the downstream channel to observe the effects (Figure 11G). Results showed

that inhibiting the CXCL12-CXCR4 connection led to the lowest percentage of adhesion. This experiment showed not only a microfluidic device capable of replicating a microenvironment resembling breast cancer adhesion to the human vasculature, but also showed that disabling certain chemokine connections may prove to be an important step towards the regulation of metastasis.

Cancer migration to bone is another scenario that has been researched. Bersini et al.[8] created a microfluidic system to look at the interaction between breast cancer cells within a microenvironment used to represent bone structure. The device uses 3 microchannels with 8 hydrogel regions within 4 hydrogel channels. Culture media flows through the 3 microchannels, with HUVEC cells cultivated in the central channel. Cultivated hBM-MSC bone marrow cells within a collagen type 1 solution were injected into the 4 hydrogel channels structured with ECM. This produced an osteo-cell region within the hydrogel channel. After 3 days of cultivation, breast cancer cells (MDA-MB-231) were introduced to the system. Trials focused on observing the cross-talk between the osteo-cell regions and the breast cancer cells. Specifically, the interactions of CXCL5, a chemokine derived from the hBM-MSC, and the CXCR2 receptor from MDA-MB-231. Results showed that in comparison to a gel only region (38%), the osteo-cell hydrogel region contained more transmigrated cancer cells (78%). These cancer cells were also able to penetrate deeper into the osteo-cell microenvironment. Additionally, the transmigrated cells showed signs of proliferation within the osteo-cell region. These proliferated cancer cells formed in clumps ranging from 4–60 cells. These results were successful in showing a functional cancer-bone cross-talk environment. Additionally, their environment promoted cancer cell transmigration, both in quantity and depth. Taking this into account, along with the observations of cancer cell metastasis within the osteo-cell region after transmigration, it is clear that the osteo-cell region provided a suitable environment for cancer cells.

A design focused on the extravasation of cancer cells through an endothelial barrier was developed by Jeon et al.[77] Similar to the previous design, this design contained three microfluidic channels with hydrogel compartments separating each channel. These hydrogel compartments contained an ECM structure. Human microvascular endothelial cells (hMVECs) were seeded within the central channel and cultured in the device. The cell line MDA-MB-231 was used to represent the tumor cells. These cells were also introduced into the central challenge after a confluent monolayer of hMVEC cells were formed. Results showed a successful extravasation of tumor cells through the endothelial barrier, with signs of proliferation in the ECM gel. Additionally, it was found that the number of extravasated cells stagnated after the first day, in agreement with in vivo studies.

2.7.5. Multiple Organs

As briefly discussed earlier in this paper, organ-on-a-chip technology can be applied to a system of multiple organs, and sometimes dubbed "human-on-a-chip," depending on how large of a portion of the human body the device represents. This has been the focal point to some research topics.[78] Multiple organs-on-

a-chip provide their own challenges mainly due to their complexity. Organ-organ interactions themselves add another layer of complexity to the system.[79]

Scaling from a multiple organ-on-a-chip in order to apply to in vivo humans is a challenge in and of itself.[80] Before body-on-a-chip systems can be implemented, consideration of the scaling effect between these micro-representations of organs with their actual in vivo counterparts must be done. Wikswo et al.[80a] broke this idea down into several groups.

First, an allometric scaling can be done to represent organs. Because humans scale allometrically, scaling differences between interconnected organ-on-a-chip systems provide an especially difficult challenge for researchers. Not only would scaling involve considerations for the mass allometrics of the organs, but properties such as blood circulation and pulse would also be affected by scaling. Another consideration would be the aspects and properties of organs that are independent of size, which may fail or become dysfunctional when scaled.

The second approach towards dealing with scaling is considering the human-on-a-chip as only a portion of the human body, dubbed "histological sections". In this respect, scaling considerations become unnecessary. The design can be such that the designed section of the organ only needs to perform the physiological duties associated with that section, eliminating some of the complexity of mimicking in vivo organs. Issues can arise when combining these sections due to either misrepresenting the organ-organ interactions by not considering the effects of a missing section of one of the organs or by not accounting for the scales of the sections relative to each other.

The third approach is to scale with consideration to organ functions. In other words, the preservation of the important organ functions is paramount when scaling in this respect. The drawback for this approach is that it may oversimplify the design to the point where various results aren't translatable.

Work done by Zhang et al.,[81] combined a multi-channel three dimensional cell culture system with compartments for different cells. Four different organs were tested in this system: C3A cells (liver), A549 cells (lung), HK-2 cells (kidney) and HPA cells (fat). All organs were connected and a "common medium" (CM) was created to keep the functions of each individual cell line. Results showed that all but the HK-2 cells were able to function at expected levels, with HK-2 functionality decreased 10%. Despite this shortcoming, the medium was deemed suitable for the experiment. The cells were connected to a reservoir containing the medium, with connections to an inlet directly attached to each cell group. The effects of TGF-β1 were tested in the multi-chip. Results showed that it did have the capabilities of promoting cell growth in A549, HK-2, and HPA cells. However, it also resulted in a much lower viability of C3A cells. To counteract this effect, gelatin microspheres were fabricated, with the ability to control the release of TGF-β1 so that it is only delivered in the A549 cell group. The results showed that A549 cells were indeed stimulated without adverse effects to any other cells. This experiment is capable of testing the multi-organ implications from drug toxicity testing.

A microscale cell culture analog (μCCA) based on a pharmacokinetic-pharmacodynamic (PK-PD) mathematical model has also been explored as a means to create a "body-on-a-chip".[82] This model has the potential to be able to mathematically
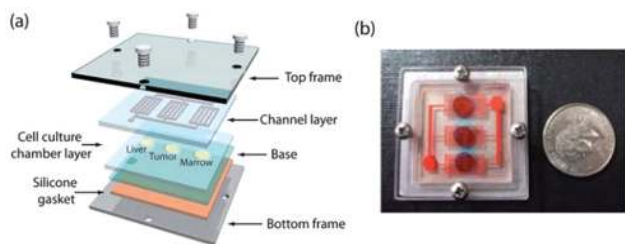
Figure 12. Layout of the device, showing A) the layer-by-layer design, and B) the image of the assembled device, with a quarter for scale. Reproduced with permission.[83] Copyright 2010, The Royal Society of Chemistry.

predict and map out the pharmacological effects of a drug. Sung et al.[83] tested the capabilities of PK-PD modeling with a multiorgan chip device designed to test drug toxicity. Three different cell lines were cultivated in separate cell culture chambers: HepG2/C3A (liver), HCT-116 (tumor), and Kasumi-1 (marrow). A reservoir containing suitable medium is fed into the three cell culture chambers. Flow was induced through a rocking motion, allowing gravity to control the flow rate. This devices changes course every 3 min, ensuring that good viability is maintained throughout the device. Layout of the device can be seen in **Figure 12**. Trials were done in which 5-fluorouracil (5-FU), an anti-cancer drug, was introduced into the medium. Different trials were done at varying concentrations. Both PK-PD modeling and experimental testing were done to observe the results. Results from experimental data show similar trends. Further trials were conducted using both 5-FU and uracil, which is known as a modulator of 5-FU. Results showed a decline in viability between all three cell groups. Through this experiment, PK-PD modeling and microfluidic multi-organ functionality were combined to test the functionality when introduced to a drug test. The results obtained from this experiment are promising, and may lead to future studies in this area.

A sample design of a body-on-a-chip was designed using chips discussed in this paper (**Figure 13**). When inter-connecting organ-on-a-chips, it is vital to recognize which organs must interact with others, and conversely, which organs must be separated from others. The medium introduced must be able to interact with the various cells without harming them.

3. Conclusions

Organ-on-a-chip systems are still a relatively new area of research, but have shown the potential to produce successful results with few caveats. For this reason, it is important to be able to expand the horizon with these

systems and explore new ideas within this area. In a broader sense, this research promotes the exploration of cheap, reliable alternatives to other forms of drug testing. Organ-on-a-chip designs have the potential to be mass produced and use few amounts of materials. This would have the potential of being used universally, including underdeveloped countries.

However, there are still steps needed to be taken in order to reach this level of reliability. While most tests have shown the ability to mimic organ functions and reactions, these are still not at the level to be a successful alternative to in vivo studies. Issues with inducing all the potential mechanical forces, achieving respectable permeation rates, producing efficient flow through polymer compartments, and recreating the microscale ecosystem of organisms, cells, bacteria that are relevant to the function of the organs, are considerations that require continued improvement. Additionally, single organ studies neglect to consider the implications that other organs within the same flow would have on that organ. Body-on-a-chip studies show great promise in this respect, but issues with components positively effecting one culture and negatively affecting another must be corrected. Methods like creating a gelatin microsphere
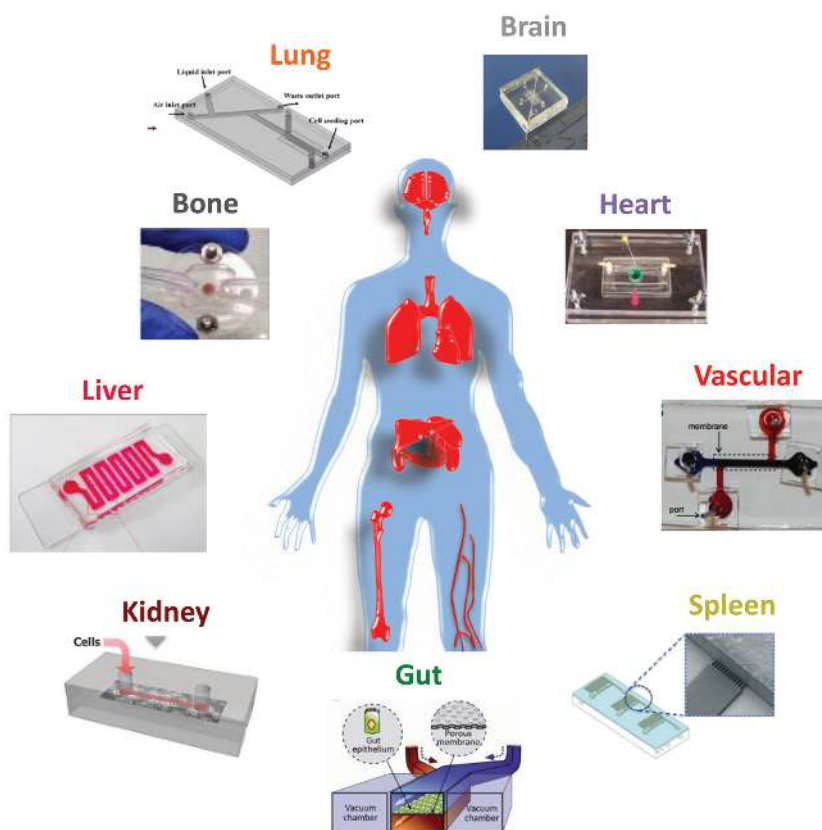
Figure 13. Sample construction of a body-on-a-chip using microfluidic chips discussed in this paper. Drug testing would begin at the lung or gut, with the liver only accessible through the gut. From there, the flow would travel in the blood, reaching the kidney, heart, bone marrow, brain, spleen, and vasculature. Reproduced with permission: lung,[26] Copyright 2011, Springer; gut,[40] Copyright 2012, The Royal Society of Chemistry; liver,[16] Copyright 2013, Elsevier; kidney,[50] Copyright 2013, The Royal Society of Chemistry; heart,[58] Copyright 2010, American Chemical Society; bone marrow,[67] Copyright 2014, Nature Publishing Group; brain,[69] Copyright 2012, Springer; spleen,[70] Copyright 2014, The Royal Society of Chemistry; and vasculature,[66] Copyright 2011, American Institute of Physics.

www.MaterialsViews.com

ADVANCED
HEALTHCARE
MATERIALS

www.advhealthmat.de

REVIEW

Table 1. Categorizes each work based on the type of organ, type of testing, details of the design and experiments, and the cells used.

Organ	Type of testing	Details	Cultured cells in device	Ref.
Liver	Toxicity/Drug Testing	Created 3D HepaTox Chip for hepatotoxicity testing	Harvested rat hepatocytes	[13]
		Encapsulated hepatocytes in 3D microtissues to study the interactions of drugs	Harvested rat hepatocytes	[12a]
		MODS platform for hepatotoxicity screening	HepG2 and NIH-3T3	[17b]
		Characterizing the toxicity of several compounds using liver co-culture and SMART-scale analysis	HepG2/C3A and MDCK	[20]
		Drug metabolism using liver and intestinal slices	Harvested rat liver and intestinal slices	[22]
		Testing the effects of ethanol-induced toxicity on liver slices	Harvested rat liver slices	[21]
	Functional analysis	Creating model with bile canaliculi formation	Harvested rat hepatocytes	[14]
		Incorporated biosensors for pH monitoring in chip	HepG2	[15]
		The kinetic reactions representing metabolism, measured and compared with mathematical model	Harvested rat liver microsomes	[16]
		Liver sinusoid pattern assembly through use of dielectrophoresis	Primary human hepatocytes and endothelial cells	[18]
		Mimicking of the acinus function in the liver	Hepatocytes and nonparenchymal cells	[17a]
		Liver and skin co-culture used to test long-term functionality under	HHSteC and skin biopsies	[19]
		Created IIDMP to evaluate dynamic organ-organ interactions of the liver and intestine	HepG2/C3A and Caco-2 TC7	[23]
Lung	Toxicity/Drug Testing	Modeling disease functions through a chip undergoing cyclic mechanical strain	Human alveolar epithelial/microvascular endothelial cells	[27]
		Cellular response and resistance to anticancer drug testing	SK-MES-1	[32]
		Modeling the nasal epithelium for formaldehyde toxicity testing	NIH/3T3 and hNESPC	[34]
	Functional analysis	Representing pulmonary diseases through propagating liquid plugs	SAEC	[25]
		Analysis of the role of surfactants in liquid plug injury	A549, ATCC	[26]
		Testing the transport properties with physiological "breathing" chip design	Human alveolar epithelial/microvascular endothelial cells	[7]
		Observing cellular injury through both solid and fluid mechanical stress	A549, AEC	[28]
		Producing suitable levels of gas transfer for artificial lung applications	N/A	[29]
		Gaseous exchange in vascular network through creation of free-standing membranes	N/A	[31]
		Optimizing flow and gaseous exchange through use of a vascular scaffold	N/A	[30]
Intestine	Toxicity/Drug Testing	µCCA model to study GI tract and predict drug toxicity	Caco-2 and HepG2/C3A	[36]
		Testing drug permeability in the intestinal epithelial cell membrane through use of microhole trapping	Caco-2	[44]
	Functional analysis	Use of hydrogels as a platform for cultivated cells in a GI tract design	Caco-2	[38]
		Functional model for potential integration in a body-on-a-chip design	Caco-2	[37a]
		Compound analysis through pH control with respect to GI tract activity	N/A	[37b]
		Mimicking the function of mucus secretion in the stomach	N/A	[37c]
		Characterizing flow and transport properties of the intestines using a villi scaffold	Caco-2	[37d]
		Modeling lipid digestion in various gastrointestinal conditions	N/A	[37e]
		Analyzing signals through bacteria-cell interaction in GI tract	HeLa S3	[39]

ADVANCED
HEALTHCARE
MATERIALS
www.advhealthmat.de

Materials Views
www.MaterialsViews.com

REVIEW

Table 1. Continued

Organ	Type of testing	Details	Cultured cells in device	Ref.
		Utilizing mechanical stress and microbes in a gut-on-a-chip	Caco-2	[40]
		Generation of 3D intestinal villi through introduction of mechanical stress	Caco-2	[41]
		Use of polarized cells to create microenvironment suited for long-term perfusion	Caco-2	[42]
		Testing the permeation abilities and intestinal absorption through microfluidics	Caco-2	[43]
Kidney	Toxicity/Drug Testing	Testing the effects of drugs on the proliferation of a dynamic kidney microfluidic chip	MDCK	[47]
		Exposure to fluid flow to create functionality and measure nephrotoxicity activity	Human kidney proximal tubular epithelial cells	[50]
	Functional analysis	Using optical vortices to enhance the functions of a blood cleaner-on-a-chip	N/A	[46a]
		Fabricating a nanofiber membrane for filtration in a microfluidic design	N/A	[46b]
		Analyzing the gene and protein expression in MDCK cells	MDCK	[46c]
		Role of patterned membrane in renal chip function	HK-2 and RPTEC	[46d]
		Use of adipose-derived stem cells in enhancing renal properties and functions	MDCK and CG-ASC	[46e]
		Utilization of fluid shear stress to enhance renal functions	IMCD	[48]
		Collecting duct-on-a-chip to investigate the effects of changes within a renal environment	IMCD	[49]
		MTMD capable of utilizing fluid shear stress and topographical patterns	HK-2	[51]
		Using TEER measurements to analyze a working kidney bioreactor under fluid shear stress conditions	HREC and MDCK	[52]
		Analyzing filtration for mass transfer capabilities modeling a glomerular unit	N/A	[53]
		Investigation of the properties of mass transfer and drug transport in MDCK cells	MDCK	[54]
Heart	Functional analysis	Studying the contraction of a single cardiomyocyte	Harvested rabbit heart tissue	[57a]
		Measurements conducted through electrode array analyzing a functioning cardiomyocyte	Harvested rabbit ventricular myocytes	[57b]
		Effects of myocardial injury in a micropillar array environment	H9C2	[57c]
		Reconstituting Barth's syndrome through a functional heart-on-a-chip	iPSC-CM	[57d]
		Studying the functions of skeletal myoblasts for myocardial injury	H9C2 and L6 myoblasts	[57e]
		Replicating physical loading in the left ventricle through a μCCCM	H9C2	[58]
		Fabrication of micro spherical pump made from cardiomyocytes	Rat cardiomyocyte cells	[60]
		TSM sensor for acoustic wave analysis of cardiomyocyte contractions	Rat ventricular cardiomyocytes	[61]
		SVF method for organ tissue analysis	Chick heart	[62]
Vasculature	Functional analysis	Implantable microfluidic device for formation of vasculature	hEPC	[64a]
		Studying the effects of the architecture in the vasculature through ECM distribution	HUVEC	[64b]
		Creation of vasculature network through material fracture	N/A	[64c]
		Establishing vasculature transport for use in multi-organ applications	HDMEC	[64d]
		Creating diffusive vasculature network from hydrogel	pHUVEC	[64e]

www.MaterialsViews.com

ADVANCED
HEALTHCARE
MATERIALS
www.advhealthmat.de

REVIEW

Table 1. Continued

Organ	Type of testing	Details	Cultured cells in device	Ref.
		Using TEMS to replicate vasculature environment	HUVEC, hCMEC/D3, BT-474/PC3	[64f]
		Bifurcating microchannel vasculature network with circular cross-sections	HUVEC	[65]
		Effects of shear stress, monocyte-EC adhesion, and monocyte transmigration on a vasculature system	PAEC, RAW264.7, THP-1	[66]
Bone Marrow	Toxicity/Drug Testing	Radiation-induced toxicity effects on a bone marrow-on-a-chip	hematopoietic and adipocyte cells	[67]
Cancer/Tumor	Toxicity/Drug Testing	Studying chemotherapy resistance using a lung cancer microfluidic model	SPCA1	[71a]
		Effects of anticancer drugs on lung and stromal cells	SPCA1 and HFL1	[71b]
		Analysis of CTCs in multiple lung cancer cell lines	A459, SK-MES-1, and H446	[71c]
		Analysis of chemotherapy resistance and inhibitors for lung cancer model	SPCA1	[71d]
		Observing the effects of various drugs on breast cancer cells through a droplet microfluidic device	MDC-MB-231	[72d]
	Functional analysis	MMICH platform for diagnosis of breast cancer	AU-565, SK-BR-3, HCC70, and MCF-7	[72a]
		Detection of breast cancer recurrence using PDMAEMA	N/A	[72b]
		Modeling the transition from DCIS to IDC for breast cancer analysis	MCF-DCIS and HMF	[72c]
		CTC capture and analysis for prostate cancer in a GEDI device	U937, PC-3, LNCaP, and C4–2	[73a]
		EIS biosensor for prostate cancer screening	N/A	[73b]
		Separation of prostate cancer cells from white blood cells using acoustophoresis	DU145, PC3, LNCaP	[73c]
		Recreating prostate cancer microenvironment using fluid shear stress	PC-3	[73d]
		Analysis of CTC in pancreatic cancer cell line	MCF-7, Hs578T, and SW620	[74]
		Using an MCS for characterization of brain cancer cells	A172, 1321N1, L0329, and L0367	[75]
		Replicating the functionalities of breast cancer cells in a vasculature system	HDMEC and MDA-MB-231	[76]
		Observing the effects of breast cancer cells within a bone structure microenvironment	HUVEC, hBM-MSC, and MDA-MB-231	[8]
		Extravasation of cancer cells through an endothelial barrier	hMVEC and MDA-MB-231	[77]
Brain	Toxicity/Drug Testing	Drug permeability testing through the BBB	HUVEC	[68c]
	Functional analysis	Creation and utilization of a SyM-BBB to monitor tight junctions and permeability	RBE4	[68a]
		Analysis of μBBB device to replicate permeability and cell characteristics	b.END3 and C8D1A	[68b]
		Integrating collagen into BBB model capable of permeability and shear stress analysis	Endothelial cell, pericyte, and astroglia	[68d]
		Use of TEER measurements to test functionality of BBB-on-a-chip	hCMEC/D3	[69]
Spleen	Functional analysis	Fast-flow/Slow-flow device for testing deformability of RBC in the spleen model	N/A	[70]
Multiple Organs	Toxicity/Drug Testing	Multi-cell design for monitoring glucose concentration in the presence of various metabolites	Omental adipose tissue, HUVEC, and HepG2	[78b]
		Monitoring the multi-organ implications from drug toxicity testing	C3A, A549, HK-2, and HPA	[81]
		Testing toxicity effects on multi-cell device complete with a hydrogel structural microenvironment	HCT-116, GepG2/C3A, and Kasumi-1	[82b]
		μCCA based on PK-PD model to predict pharmacological effects of a drug	HCT-116, GepG2/C3A, and Kasumi-1	[83]
	Functional analysis	Hanging drop technique for fabrication of multi-cell device	HCT-116 eGFP and rLiMT	[78a]

for time-release drugs or providing a common medium to the system have shown promise as a way to integrate multiple cell cultures.

In this Review, individual organs are analyzed, with attention brought to their design, materials, objectives, and results (**Table 1**). Additionally, multi-organ systems are discussed, with a sample model of a "body-on-a-chip" created using designs mentioned in this paper. While it may not be as straightforward as simply connecting the designs with one another, this construction of a body-on-a-chip shows that the ability to create a successful body-on-a-chip is not inconceivable with successful designs of individual organs.

[1] a) U. Marx, H. Walles, S. Hoffmann, G. Lindner, R. Horland, F. Sonntag, U. Klotzbach, D. Sakharov, A. Tonevitsky, R. Lauster, *Altern. Lab. Anim.* **2012**, *40*, 235–257; b) C. Moraes, G. Mehta, S. C. Lesher-Perez, S. Takayama, *Ann. Biomed. Eng.* **2012**, *40*, 1211–1227.

[2] a) E. Cukierman, R. Pankov, D. R. Stevens, K. M. Yamada, *Science* **2001**, *294*, 1708–1712; b) N. Annabi, A. Tamayol, J. A. Uquillas, M. Akbari, L. E. Bertassoni, C. Cha, G. Camci-Unal, M. R. Dokmeci, N. A. Peppas, A. Khademhosseini, *Adv. Mater.* **2014**, *26*, 85–124.

[3] a) M. Odijk, A. D. Van der Meer, L. D. , H. J. Kim, M. W. van der Helm, L. I. Segerink, J. P. Frimat, G. A. Hamilton, D. E. Ingber, A. Van den Berg, *Lab Chip* **2014**; b) N. Hashemi, J. S. Erickson, J. P. Golden, F. S. Ligler, *Biomicrofluidics* **2011**, *5*, 032009; c) N. Hashemi, J. P. B. Howell, J. S. Erickson, J. P. Golden, F. S. Ligler, *Lab Chip* **2010**, *10*, 1952–1959; d) N. Hashemi, J. S. Erickson, J. P. Golden, K. M. Jackson, F. S. Ligler, *Biosens. Bioelectron.* **2011**, *26*, 4263–4269; e) D. Chen, R. D. Hyldahl, R. C. Hayward, *Lab Chip* **2015**, *15*, 1160–1167.

[4] P. Neuzil, S. Giselbrecht, K. Lange, T. J. Huang, A. Manz, *Nat. Rev. Drug Discovery* **2012**, *11*, 620–632.

[5] a) J. El-Ali, P. K. Sorger, K. F. Jensen, *Nature* **2006**, *442*, 403–411; b) D. Sechi, B. Greer, J. Johnson, N. Hashemi, *Anal. Chem.* **2013**, *85*, 10733–10737.

[6] A. O. Stucki, J. D. Stucki, S. R. R. Hall, M. Felder, Y. Mermoud, R. A. Schmid, T. Geiser, O. T. Guenat, *Lab Chip* **2015**, *15*, 1302–1310.

[7] D. Huh, B. D. Matthews, A. Mammoto, M. Montoya-Zavala, H. Y. Hsin, D. E. Ingber, *Science* **2010**, *328*, 1662–1668.

[8] S. Bersini, J. S. Jeon, G. Dubini, C. Arrigoni, S. Chung, J. L. Charest, M. Moretti, R. D. Kamm, *Biomaterials* **2014**, *35*, 2454–2461.

[9] a) R. de Kanter, P. Olinga, M. H. de Jager, M. T. Merema, D. K. F. Meijer, G. M. M. Groothius, *Toxicol. In Vitro* **1999**, *13*, 737–744; b) N. Kaplowitz, *Drug Saf.* **2001**, *24*, 483–490.

[10] R. Baudoin, A. Corlu, L. Griscom, C. Legallais, E. Leclerc, *Toxicol. In Vitro* **2007**, *21*, 535–544.

[11] C. Guguen-Guillouzo, A. Guillouzo, in *General Review on In Vitro Hepatocyte Models and Their Applications*, Vol. 640 (Ed. P. Maurel), Humana Press Inc, Totowa **2010**, pp. 1–40.

[12] a) C. Y. Li, K. R. Stevens, R. E. Schwartz, B. S. Alejandro, J. H. Huang, S. N. Bhatia, *Tissue Eng., Part A* **2014**, *20*, 2200–2212; b) S. S. Bale, L. Vernetti, N. Senutovitch, R. Jindal, M. Hegde, A. Gough, W. J. McCarty, A. Bakan, A. Bhushan, T. Y. Shun, I. Golberg, R. DeBiasio, O. B. Usta, D. L. Taylor, M. L. Yarmush, *Exp. Biol. Med.* **2014**, *239*, 1180–1191.

[13] Y. C. Toh, T. C. Lim, D. Tai, G. F. Xiao, D. van Noort, H. R. Yu, *Lab Chip* **2009**, *9*, 2026–2035.

[14] Y. Nakao, H. Kimura, Y. Sakai, T. Fujii, *Biomicrofluidics* **2011**, *5*.022212-1–022212-7.

[15] A. Schober, U. Fernekorn, B. Lubbers, J. Hampl, F. Weise, G. Schlingloff, M. Gebinoga, M. Worgull, M. Schneider, C. Augspurger, C. Hildmann, M. Kittler, M. Donahue, *Materialwiss. Werkstofftech.* **2011**, *42*, 139–146.

[16] J. Lee, S. H. Kim, Y. C. Kim, I. Choi, J. H. Sung, *Enzyme Microb. Technol.* **2013**, *53*, 159–164.

[17] a) A. Bhushan, N. Senutovitch, S. S. Bale, W. J. McCarty, M. Hegde, R. Jindal, I. Golberg, O. B. Usta, M. L. Yarmush, L. Vernetti, A. Gough, A. Bakan, T. Y. Shun, R. DeBiasio, D. L. Taylor, *Stem Cell Res. Ther.* **2013**, *4*, 1–6; b) S. H. Au, M. D. Chamberlain, S. Mahesh, M. V. Sefton, A. R. Wheeler, *Lab Chip* **2014**, *14*, 3290–3299.

[18] J. Schutte, B. Hagmeyer, F. Holzner, M. Kubon, S. Werner, C. Freudigmann, K. Benz, J. Bottger, R. Gebhardt, H. Becker, M. Stelzle, *Biomed. Microdevices* **2011**, *13*, 493–501.

[19] I. Wagner, E. M. Materne, S. Brincker, U. Sussbier, C. Fradrich, M. Busek, F. Sonntag, D. A. Sakharov, E. V. Trushkin, A. G. Tonevitsky, R. Lauster, U. Marx, *Lab Chip* **2013**, *13*, 3538–3547.

[20] L. Shintu, R. Baudoin, V. Navratil, J. M. Prot, C. Pontoizeau, M. Defernez, B. J. Blaise, C. Domange, A. R. Pery, P. Toulhoat, C. Legallais, C. Brochot, E. Leclerc, M. E. Dumas, *Anal. Chem.* **2012**, *84*, 1840–1848.

[21] S. M. Hattersley, J. Greenman, S. J. Haswell, *Biomed. Microdevices* **2011**, *13*, 1005–1014.

[22] P. M. van Midwoud, M. T. Merema, E. Verpoorte, G. M. M. Groothuis, *Lab Chip* **2010**, *10*, 2778–2786.

[23] T. Bricks, P. Paullier, A. Legendre, M. J. Fleury, P. Zeller, F. Merlier, P. M. Anton, E. Leclerc, *Toxicol. In Vitro* **2014**, *28*, 885–895.

[24] J. E. Nichols, J. A. Niles, S. P. Vega, J. Cortiella, *Stem Cell Res. Ther.* **2013**, *4*, 1–5.

[25] D. Huh, H. Fujioka, Y. C. Tung, N. Futai, R. Paine, J. B. Grotberg, S. Takayama, *Proc. Natl. Acad. Sci. U.S.A.* **2007**, *104*, 18886–18891.

[26] H. Tavana, P. Zamankhan, P. J. Christensen, J. B. Grotberg, S. Takayama, *Biomed. Microdevices* **2011**, *13*, 731–742.

[27] D. Huh, D. C. Leslie, B. D. Matthews, J. P. Fraser, S. Jurek, G. A. Hamilton, K. S. Thorneloe, M. A. McAlexander, D. E. Ingber, *Sci. Transl. Med.* **2012**, *4*, 1–8.

[28] N. J. Douville, P. Zamankhan, Y. C. Tung, R. Li, B. L. Vaughan, C. F. Tai, J. White, P. J. Christensen, J. B. Grotberg, S. Takayama, *Lab Chip* **2011**, *11*, 609–619.

[29] T. Kniazeva, J. C. Hsiao, J. L. Charest, J. T. Borenstein, *Biomed. Microdevices* **2011**, *13*, 315–323.

[30] D. M. Hoganson, H. I. Pryor, E. K. Bassett, I. D. Spool, J. P. Vacanti, *Lab Chip* **2011**, *11*, 700–707.

[31] R. Sreenivasan, E. K. Bassett, D. M. Hoganson, J. P. Vacanti, K. K. Gleason, *Biomaterials* **2011**, *32*, 3883–3889.

[32] W. Siyan, Y. Feng, Z. Lichuan, W. Jiarui, W. Yingyan, J. Li, L. Bingcheng, W. Qi, *J. Pharm. Biomed. Anal.* **2009**, *49*, 806–810.

[33] N. L. Jeon, S. K. W. Dertinger, D. T. Chiu, I. S. Choi, A. D. Stroock, G. M. Whitesides, *Langmuir* **2000**, *16*, 8311–8316.

[34] W. Wang, Y. Yan, C. W. Li, H. M. Xia, S. S. Chao, D. Y. Wang, Z. P. Wang, *Lab Chip* **2014**, *14*, 677–680.

www.MaterialsViews.com

ADVANCED
HEALTHCARE
MATERIALS

www.advhealthmat.de

REVIEW

[35] U. Fagerholm, M. Johansson, H. Lennernas, *Pharm. Res.* **1996**, *13*, 1336–1342.

[36] G. J. Mahler, M. B. Esch, R. P. Glahn, M. L. Shuler, *Biotechnol. Bioeng.* **2009**, *104*, 193–205.

[37] a) M. B. Esch, J. H. Sung, J. Yang, C. H. Yu, J. J. Yu, J. C. March, M. L. Shuler, *Biomed. Microdevices* **2012**, *14*, 895–906; b) K. Morimoto, S. Yamaguchi, J. Fukuda, H. Suzuki, *J. Appl. Phys.* **2009**, *105*, 102013-1–102013-7; c) L. Li, O. Lieleg, S. Jang, K. Ribbeck, J. Han, *Lab Chip* **2012**, *12*, 4071–4079; d) S. H. Kim, J. W. Lee, I. Choi, Y. C. Kim, J. B. Lee, J. H. Sung, *J. Nanosci. Nanotechnol.* **2013**, *13*, 7220–7228; e) S. Marze, H. Algaba, M. Marquis, *Food Funct.* **2014**, *5*, 1481–1488.

[38] J. H. Sung, J. J. Yu, D. Luo, M. L. Shuler, J. C. March, *Lab Chip* **2011**, *11*, 389–392.

[39] J. Kim, M. Hegde, A. Jayaraman, *Lab Chip* **2010**, *10*, 43–50.

[40] H. J. Kim, D. Huh, G. Hamilton, D. E. Ingber, *Lab Chip* **2012**, *12*, 2165–2174.

[41] H. J. Kim, D. E. Ingber, *Integr. Biol.* **2013**, *5*, 1130–1140.

[42] H. Kimura, T. Yamamoto, H. Sakai, Y. Sakai, T. Fujii, *Lab Chip* **2008**, *8*, 741–746.

[43] Y. Imura, Y. Asano, K. Sato, E. Yoshimura, *Anal. Sci.* **2009**, *25*, 1403–1407.

[44] J. H. Yeon, J. K. Park, *Anal. Chem.* **2009**, *81*, 1944–1951.

[45] L. Condorelli, I. Cattaneo, C. Arrigoni, L. Antiga, N. Perico, A. Remuzzi in *Effect of fluid shear stress on tubular kidney epithelial cell structure*, Vol. 25 (Eds: O. Dossel, W. C. Schlegel), Springer, New York **2009**, pp 50–52.

[46] a) N. Suwanpayak, M. A. Jalil, M. S. Aziz, F. D. Ismail, J. Ali, P. P. Yupapin, *Int. J. Nanomed.* **2011**, *6*, 957–964; b) K. H. Lee, D. J. Kim, B. G. Min, S. H. Lee, *Biomed. Microdevices* **2007**, *9*, 435–442; c) L. C. Snouber, F. Letourneur, P. Chafey, C. Broussard, M. Monge, C. Legallais, E. Leclerc, *Biotechnol. Prog.* **2012**, *28*, 474–484; d) E. M. Frohlich, J. L. Alonso, J. T. Borenstein, X. Zhang, M. A. Arnaout, J. L. Charest, *Lab Chip* **2013**, *13*, 2311–2319; e) H. C. Huang, Y. J. Chang, W. C. Chen, H. I. C. Harn, M. J. Tang, C. C. Wu, *Tissue Eng., Part A* **2013**, *19*, 2024–2034.

[47] R. Baudoin, L. Griscom, M. Monge, C. Legallais, E. Leclerc, *Biotechnol. Prog.* **2007**, *23*, 1245–1253.

[48] K. J. Jang, K. Y. Suh, *Lab Chip* **2010**, *10*, 36–42.

[49] K. J. Jang, H. S. Cho, D. H. Kang, W. G. Bae, T. H. Kwon, K. Y. Suh, *Integr. Biol.* **2011**, *3*, 134–141.

[50] K. J. Jang, A. P. Mehr, G. A. Hamilton, L. A. McPartlin, S. Y. Chung, K. Y. Suh, D. E. Ingber, *Integr. Biol.* **2013**, *5*, 1119–1129.

[51] E. M. Frohlich, X. Zhang, J. L. Charest, *Integr. Biol.* **2012**, *4*, 75–83.

[52] N. Ferrell, R. R. Desai, A. J. Fleischman, S. Roy, H. D. Humes, W. H. Fissell, *Biotechnol. Bioeng.* **2010**, *107*, 707–716.

[53] A. Ould-Dris, P. Paullier, L. Griscom, C. Legallais, E. Leclerc, *J. Membr. Sci.* **2010**, *352*, 116–125.

[54] C. Ramello, P. Paullier, A. Ould-Dris, M. Monge, C. Legallais, E. Leclerc, *Toxicol. In Vitro* **2011**, *25*, 1123–1131.

[55] a) A. Agarwal, J. A. Goss, A. Cho, M. L. McCain, K. K. Parker, *Lab Chip* **2013**, *13*, 3599–3608; b) A. Grosberg, P. W. Alford, M. L. McCain, K. K. Parker, *Lab Chip* **2011**, *11*, 4165–4173; c) A. Grosberg, A. P. Nesmith, J. A. Goss, M. D. Brigham, M. L. McCain, K. K. Parker, *J. Pharmacol. Toxicol. Methods* **2012**, *65*, 126–135; d) M. L. McCain, A. Agarwal, H. W. Nesmith, A. P. Nesmith, K. K. Parker, *Biomaterials* **2014**, *35*, 5462–5471.

[56] a) A. Mol, N. J. B. Driessen, M. C. M. Rutten, S. P. Hoerstrup, C. V. C. Bouten, F. P. T. Baaijens, *Ann. Biomed. Eng.* **2005**, *33*, 1778–1788; b) M. A. A. van Vlimmeren, A. Driessen-Mol, C. W. J. Oomens, F. P. T. Baaijens, *Tissue Eng., Part C* **2011**, *17*, 983–991; c) S. P. Hoerstrup, A. Kadner, S. Melnitchouk, A. Trojan, K. Eid, J. Tracy, R. Sodian, J. F. Visjager, S. A. Kolb, J. Grunenfelder, G. Zund, M. I. Turina, *Circulation* **2002**, *106*, I143–I150; d) A. Weymann, T. Radovits, B. Schmack, S. L. Li, S. Korkmaz, P. Soos, R. Istok, G. Veres, N. Chaimow, M. Karck, G. Szabo, *Artif. Organs* **2014**, *38*, E118–E128; e) J. Dube, J. M. Bourget, R. Gauvin, H. Lafrance, C. J. Roberge, F. A. Auger, L. Germain, *Acta Biomater.* **2014**, *10*, 3563–3570; f) S. Hinderer, J. Seifert, M. Votteler, N. Shen, J. Rheinlaender, T. E. Schaffer, K. Schenke-Layland, *Biomaterials* **2014**, *35*, 2130–2139.

[57] a) X. J. Li, P. C. H. Li, in *Contraction study of a single cardiac muscle cell in a microfluidic chip*, Vol. *321* (Ed. S. D. Minteer), Humana Press Inc, 999 Riverview Dr, Ste 208, Totowa, Nj07512–1165USA, **2006**, pp. 199–225; b) W. Cheng, N. Klauke, H. Sedgwick, G. L. Smith, J. M. Cooper, *Lab Chip* **2006**, *6*, 1424–1431; c) L. Ren, W. M. Liu, Y. L. Wang, J. C. Wang, Q. Tu, J. Xu, R. Liu, S. F. Shen, J. Y. Wang, *Anal. Chem.* **2013**, *85*, 235–244; d) G. Wang, M. L. McCain, L. H. Yang, A. B. He, F. S. Pasqualini, A. Agarwal, H. Y. Yuan, D. W. Jiang, D. H. Zhang, L. Zangi, J. Geva, A. E. Roberts, Q. Ma, J. Ding, J. H. Chen, D. Z. Wang, K. Li, J. W. Wang, R. J. A. Wanders, W. Kulik, F. M. Vaz, M. A. Laflamme, C. E. Murry, K. R. Chien, R. I. Kelley, G. M. Church, K. K. Parker, W. T. Pu, *Nat. Med.* **2014**, *20*, 616–623; e) J. He, C. Ma, W. M. Liu, J. Y. Wang, *Analyst* **2014**, *139*, 4482–4490.

[58] G. A. Giridharan, M. D. Nguyen, R. Estrada, V. Parichehreh, T. Hamid, M. A. Ismahil, S. D. Prabhu, P. Sethu, *Anal. Chem.* **2010**, *82*, 7581–7587.

[59] a) Z. Bai, H. Lin, J. Johnson, S. C. Rong Gui, K. Imakita, R. Montazami, M. Fujii, N. Hashemi, *J. Mater. Chem. C* **2014**, *2*, 1736–1741; b) H. Acar, S. Çınar, M. Thunga, M. R. Kessler, N. Hashemi, R. Montazami, *Adv. Funct. Mater.* **2014**, *24*, 4135–4143.

[60] Y. Tanaka, K. Sato, T. Shimizu, M. Yamato, T. Okano, T. Kitamori, *Lab Chip* **2007**, *7*, 207–212.

[61] P. C. H. Li, W. J. Wang, M. Parameswaran, *Analyst* **2003**, *128*, 225–231.

[62] H. Owaki, T. Masuda, T. Kawahara, K. Miyasaka, T. Ogura, F. Arai, in *Concurrent connection of embryonic chick heart using a microfluidic device for Organ-Explant-Chip*, Vol. *5* Eds.: M. Mitsuishi, P. Bartolo), Elsevier Science Bv, Amsterdam **2013**, pp 205–209.

[63] J. E. Deanfield, J. P. Halcox, T. J. Rabelink, *Circulation* **2007**, *115*, 1285–1295.

[64] a) J. Kim, K. Yang, H. J. Park, S. W. Cho, S. Han, Y. Shin, S. Chung, J. H. Lee, *Biotechnol. Bioprocess Eng.* **2014**, *19*, 379–385; b) B. M. Baker, B. Trappmann, S. C. Stapleton, E. Toro, C. S. Chen, *Lab Chip* **2013**, *13*, 3246–3252; c) J. H. Huang, J. Kim, N. Agrawal, A. P. Sudarson, J. E. Maxim, A. Jayaraman, V. M. Ugaz, *Adv. Mater.* **2009**, *21*, 3567–+; d) K. Schimek, M. Busek, S. Brincker, B. Groth, S. Hoffmann, R. Lauster, G. Lindner, A. Lorenz, U. Menzel, F. Sonntag, H. Walles, U. Marx, R. Horland, *Lab Chip* **2013**, *13*, 3588–3598; e) X. Mu, W. F. Zheng, L. Xiao, W. Zhang, X. Y. Jiang, *Lab Chip* **2013**, *13*, 1612–1618; f) A. Tourovskaia, M. Fauver, G. Kramer, S. Simonson, T. Neumann, *Exp. Biol. Med.* **2014**, *239*, 1264–1271.

[65] J. T. Borenstein, M. M. Tupper, P. J. Mack, E. J. Weinberg, A. S. Khalil, J. Hsiao, G. Garcia-Cardena, *Biomed. Microdevices* **2010**, *12*, 71–79.

[66] S. Srigunapalan, C. Lam, A. R. Wheeler, C. A. Simmons, *Biomicrofluidics* **2011**, *5*, 013409-1–013409-9.

[67] Y. S. Torisawa, C. S. Spina, T. Mammoto, A. Mammoto, J. C. Weaver, T. Tat, J. J. Collins, D. E. Ingber, *Nat. Methods* **2014**, *11*, 663-+.

[68] a) B. Prabhakarpandian, M. C. Shen, J. B. Nichols, I. R. Mills, M. Sidoryk-Wegrzynowicz, M. Aschner, K. Pant, *Lab Chip* **2013**, *13*, 1093–1101; b) R. Booth, H. Kim, *Lab Chip* **2012**, *12*, 1784–1792; c) J. H. Yeon, D. Na, K. Choi, S. W. Ryu, C. Choi, J. K. Park, *Biomed. Microdevices* **2012**, *14*, 1141–1148; d) K. Shibata, H. Terazono, A. Hattori, K. Yasuda, *Jpn. J. Appl. Phys.* **2008**, *47*, 5208–5211.

[69] L. M. Griep, F. Wolbers, B. de Wagenaar, P. M. ter Braak, B. B. Weksler, I. A. Romero, P. O. Couraud, I. Vermes, A. D. van der Meer, A. van den Berg, *Biomed. Microdevices* **2013**, *15*, 145–150.

[70] L. G. Rigat-Brugarolas, A. Elizalde-Torrent, M. Bernabeu, M. De Niz, L. Martin-Jaular, C. Fernandez-Becerra, A. Homs-Corbera, J. Samitier, H. A. del Portillo, *Lab Chip* **2014**, *14*, 1715–1724.

[71] a) L. C. Zhang, J. R. Wang, L. Zhao, Q. A. Meng, Q. Wang, *Electrophoresis* **2010**, *31*, 3763–3770; b) Z. Y. Xu, Y. H. Gao, Y. Y. Hao, E. C. Li, Y. Wang, J. N. Zhang, W. X. Wang, Z. C. Gao, Q. Wang, *Biomaterials* **2013**, *34*, 4109–4117; c) T. Huang, C. P. Jia, Y. Jun, W. J. Sun, W. T. Wang, H. L. Zhang, H. Cong, F. X. Jing, H. J. Mao, Q. H. Jin, Z. Zhang, Y. J. Chen, G. Li, G. X. Mao, J. L. Zhao, *Biosens. Bioelectron.* **2014**, *51*, 213–218; d) Q. Meng, Z. Z. He, L. C. Zhang, L. Zhao, E. C. Li, Q. Q. Zhang, X. L. Zhang, D. X. Yang, L. J. Zou, Z. C. Gao, Q. Wang, *Electrophoresis* **2011**, *32*, 3446–3453.

[72] a) M. S. Kim, T. Kim, S. Y. Kong, S. Kwon, C. Y. Bae, J. Choi, C. H. Kim, E. S. Lee, J. K. Park, *PloS One* **2010**, *5*; b) J. K. Chen, B. J. Bai, F. C. Chang, *Appl. Phys. Lett.* **2011**, *99*; c) K. E. Sung, N. Yang, C. Pehlke, P. J. Keely, K. W. Eliceiri, A. Friedl, D. J. Beebe, *Integr. Biol.* **2011**, *3*, 439–450; d) Z. C. Gong, H. Zhao, T. H. Zhang, F. Nie, P. Pathak, K. M. Cui, Z. Y. Wang, S. Wong, L. Que, *Biomed. Microdevices* **2011**, *13*, 215–219.

[73] a) B. J. Kirby, M. Jodari, M. S. Loftus, G. Gakhar, E. D. Pratt, C. Chanel-Vos, J. P. Gleghorn, S. M. Santana, H. Liu, J. P. Smith, V. N. Navarro, S. T. Tagawa, N. H. Bander, D. M. Nanus, P. Giannakakou, *PLoS One* **2012**, *7*, 1–10; b) M. S. Chiriaco, E. Primiceri, A. Montanaro, F. de Feo, L. Leone, R. Rinaldi, G. Maruccio, *Analyst* **2013**, *138*, 5404–5410; c) P. Augustsson, C. Magnusson, M. Nordin, H. Lilja, T. Laurell, *Anal. Chem.* **2012**,

84, 7954–7962; d) L. Y. Liu, K. Loutherback, D. Liao, D. Yeater, G. Lambert, A. Estevez-Torres, J. C. Sturm, R. H. Getzenberg, R. H. Austin, *Lab Chip* **2010**, *10*, 1807–1813.

[74] J. W. Kamande, M. L. Hupert, M. A. Witek, H. Wang, R. J. Torphy, U. Dharmasiri, S. K. Njoroge, J. M. Jackson, R. D. Aufforth, A. Snavely, J. J. Yeh, S. A. Soper, *Anal. Chem.* **2013**, *85*, 9092–9100.

[75] Z. S. Khan, S. A. Vanapalli, *Biomicrofluidics* **2013**, *7*, 011806-1–011806-15.

[76] J. W. Song, S. P. Cavnar, A. C. Walker, K. E. Luker, M. Gupta, Y. C. Tung, G. D. Luker, S. Takayama, *PLoS One* **2009**, *4*, 1–10.

[77] J. S. Jeon, I. K. Zervantonakis, S. Chung, R. D. Kamm, J. L. Charest, *PLoS One* **2013**, *8*, 1–9.

[78] a) O. Frey, P. M. Misun, D. A. Fluri, J. G. Hengstler, A. Hierlemann, *Nat. Commun.* **2014**, *5*, 1–11; b) E. Iori, B. Vinci, E. Murphy, M. C. Marescotti, A. Avogaro, A. Ahluwalia, *PLoS One* **2012**, 1–9.

[79] M. B. Esch, A. S. T. Smith, J. M. Prot, C. Oleaga, J. J. Hickman, M. L. Shuler, *Adv. Drug Delivery Rev.* **2014**, *69*, 158–169.

[80] a) J. P. Wikswo, E. L. Curtis, Z. E. Eagleton, B. C. Evans, A. Kole, L. H. Hofmeister, W. J. Matloff, *Lab Chip* **2013**, *13*, 3496–3511; b) C. Moraes, J. M. Labuz, B. M. Leung, M. Inoue, T. H. Chun, S. Takayama, *Integr. Biol.* **2013**, *5*, 1149–1161.

[81] C. Zhang, Z. Q. Zhao, N. A. A. Rahim, D. van Noort, H. Yu, *Lab Chip* **2009**, *9*, 3185–3192.

[82] a) J. H. Sung, B. Srinivasan, M. B. Esch, W. T. McLamb, C. Bernabini, M. L. Shuler, J. J. Hickman, *Exp. Biol. Med.* **2014**, *239*, 1225–1239; b) J. H. Sung, M. L. Shuler, *Lab Chip* **2009**, *9*, 1385–1394.

[83] J. H. Sung, C. Kam, M. L. Shuler, *Lab Chip* **2010**, *10*, 446–455.